# Parametrisation of the Cloud Topped Boundary Layer: Aircraft Measurements.

by

D.W.Johnson

Meteorological Office, Meteorological Research Flight, DRA, Farnborough, Hants GU14 6TD

**ABSTRACT:** *The effective radius of cloud droplets in warm stratocumulus clouds has been investigated by analysing observations from the Meteorological Research Flight's Hercules C-130 aircraft. Results from experiments in the Eastern Pacific, South Atlantic, sub-tropical regions of the North Atlantic and the sea areas around the British Isles are presented. In situations where entrainment effects are small the (effective radius)$^3$ is found to be a linear function of the (volume averaged radius)$^3$ in a given cloud and can thus be parametrised with respect to the liquid water content and the droplet number concentration. The shape of the droplet size spectrum is very dependent on the cloud condensation nuclei (CCN) characteristics below cloud base, and the relationship between effective radius and volume averaged radius varies between maritime airmasses and continental airmasses. This study also details comparisons that have been made in stratocumulus between the droplet number concentrations and (a) aerosol concentrations below cloud base and (b) CCN supersaturation spectra in the boundary layer. A parametrisation relating droplet concentration and aerosol concentration is suggested. Comparisons are made between this parametrisation of effective radius and others being used currently. The penetration of cumulus clouds into stratocumulus layers are observed to have a significant effect on the reflectivity of the layer clouds and interpretations of these observations are presented.*

## 1. Introduction

Stratus and stratocumulus clouds have high albedos and reduce the shortwave radiation received at the earth's surface (Albrecht *et al.* 1988, Betts and Boers 1990). These boundary layer clouds are therefore important components of the earth's energy budget. They are observed to occur in very persistent sheets covering large areas of the eastern parts of subtropical ocean basins over the cooler ocean currents found there and as more transient features under mid-latitude anticyclones (Schmetz *et al.* 1983) and in arctic regions (Curry and Herman 1985). The reflectivity of these clouds is very sensitive to their liquid water content and to the microphysical processes going on within them (Taylor and Ghan 1992). Twomey (1974) has suggested that their albedo is modified by the characteristics of the cloud condensation nuclei (CCN) available to form the cloud drops. By changing the droplet size distribution and concentration, the optical properties of the cloud may be altered sufficiently to change the global energy budget and thus the climate (Twomey 1977a, Charlson *et al.* 1987). It is therefore important that numerical weather and climate models simulate realistically the radiative properties of these clouds (Mitchell *et al.* 1989).

However, such models have too large a grid spacing to resolve explicitly the microphysical processes associated with these clouds. Therefore their effects have to be

parametrised in terms of the bulk model variables in order to improve the model predictions. The three most important parameters needed to describe the radiative properties of clouds are

**(i)** the optical thickness

**(ii)** the single scattering albedo and

**(iii)** the asymmetry factor

Stephens (1978*b*) and Slingo and Schrecker (1982) show that in liquid water clouds all three of these can be parametrised in terms of the effective radius ($r_e$) of the droplet size spectrum. The effective radius is defined as

$$r_e = \frac{\int_{r=0}^{\infty} N_r r^3 \, dr}{\int_{r=0}^{\infty} N_r r^2 \, dr} \tag{1}$$

where $r$ is the cloud droplet radius and $N$ the droplet concentration. Slingo (1990) estimated that decreasing the effective radius of cloud droplets from 10 $\mu m$ to 8 $\mu m$, which increases the shortwave albedo, would result in atmospheric cooling that could offset global warming due to doubling the $CO_2$ content of the atmosphere. Equally, Randall *et al.* (1984) have shown that this offset could also be brought about by a four percent increase in the area covered by stratocumulus. Radiation schemes used in large scale numerical models are therefore very sensitive to the effective radius. The main focus of this paper is the analysis of extensive aircraft observations of marine stratocumulus clouds from several different regions of the world in both maritime airmasses and continental airmasses which suggest a new parametrisation of effective radius for layer clouds that could be used in numerical model radiation schemes.

## 2. Aircraft instrumentation and data sets used.

The data analysed below were recorded by the Meteorological Research Flight (MRF) Hercules C-130 aircraft during

**(i)** the First ISCCP (International Satellite Cloud Climatology Program) Regional Experiment (FIRE) conducted over the eastern Pacific Ocean off the southern coast of California in July 1987,

**(ii)** the First ATSR (Along Track Scanning Radiometer) Tropical Experiment (FATE) in the South Atlantic during November 1991,

**(iii)** flights made in stratocumulus over the sea areas around the British Isles between December 1990 and February 1992, and

**(iv)** the Atlantic Stratocumulus Transition Experiment (ASTEX) carried out in the North Atlantic in the vicinity of the Azores in June 1992.

In all, data from 36 flights have been used.

Detailed information about the instrumentation used on the C-130 and its performance is given in Rogers *et al.* (1993). The instruments used to obtain the microphysical data analysed here were a Particle Measuring Systems (PMS) Passive Cavity Aerosol Spectrometer Probe (PCASP) which measures aerosol particles in the range 0.05 to 1.50 $\mu m$ radius (Strapp *et al.* 1992), a PMS Forward Scattering Spectrometer Probe (FSSP),

which measures droplets in the range 0.25 to 24 $\mu m$ radius (Baumgardner 1983), a PMS 2D cloud probe which measures droplets in the size range 12.5 to 400 $\mu m$ radius (Moss and Johnson 1993) and a thermal gradient diffusion chamber to measure CCN activity spectra (Saxena and Kassner 1970). Two basic flight patterns were used: (a) a profile, where a slow descent (500ft/min in the boundary layer, 1000ft/min in the free troposphere) was made through the cloud sampling the microphysics of the cloud and the aerosol characteristics below cloud base, and (b) a stack in which a series of 5 to 10 minute straight and level runs was performed, the first immediately below the cloud base to sample the aerosol in the boundary layer and the rest at several different heights in the cloud. The technique used for measuring the CCN supersaturation spectra is very slow so, normally, only one spectrum could be obtained below cloud base in both the profiles and the stacks.

## 3. Typical stratocumulus cloud characteristics.

Stratocumulus clouds normally form underneath a subsidence inversion over a relatively cool sea surface. Figure 1(a) shows a typical tephigram obtained during a slow descent through a layer of stratocumulus off the coast of California. The cloud which was 400m thick had formed in a moderate northerly flow in a well mixed boundary layer that was approximately 1km deep and capped by a sharp temperature inversion. As found by several other investigators (Nicholls 1984, Nicholls and Leighton 1986, Albrecht *et al.* 1988, Bower and Choularton 1992) the corresponding liquid water content profile, as shown in Figure 1(b), increases smoothly with height, with a large step change at cloud top. However, the droplet concentration (Figure 1(c)) measured by the FSSP remains almost constant throughout the depth of the cloud and there are sharp changes both at cloud base and cloud top. The average size of the droplets increases with height, as illustrated in Figure 1(d), which is a profile of the effective radius of cloud droplets. This is calculated from droplet size spectra measured by the FSSP using the following equation:

$$r_e = \frac{\sum_{n=1}^{M} r_n^3 N_n}{\sum_{n=1}^{M} r_n^2 N_n} \tag{2}$$

where M is the number of size bins resolved by the FSSP (M = 15), $r_n$ is the middle radius value for that size bin and $N_n$ is the concentration of droplets in that size bin.

The example given in Figure 1 is typical of most of the stratocumulus clouds used in this study. It is consistent with a layer of cloud having formed in a boundary layer with relatively homogeneous aerosol characteristics below cloud base and where the maximum supersaturation in the rising parcels of air is experienced just above cloud base, so that all the CCN in the parcel that are going to be activated are activated at this level. Therefore the droplet concentration remains constant throughout the depth of the cloud. Occasionally, profiles showed a decrease in mean droplet concentration close to the upper and lower cloud boundaries, with corresponding decreases in liquid water content. However, in most cases these effects were small, which indicates that entrainment in these stratocumulus clouds is not generally a significant effect, and is mainly limited to cloud top. On occasions when entrainment was noticeable, such as when cumulus clouds were penetrating the layer or when the layer was very thin or broken, the data were left out of the analysis.

The most significant microphysical variation observed in the stratocumulus clouds during the course of these experiments was the difference in shape of the droplet spectra between maritime and continental airmass clouds. The airmass type was determined

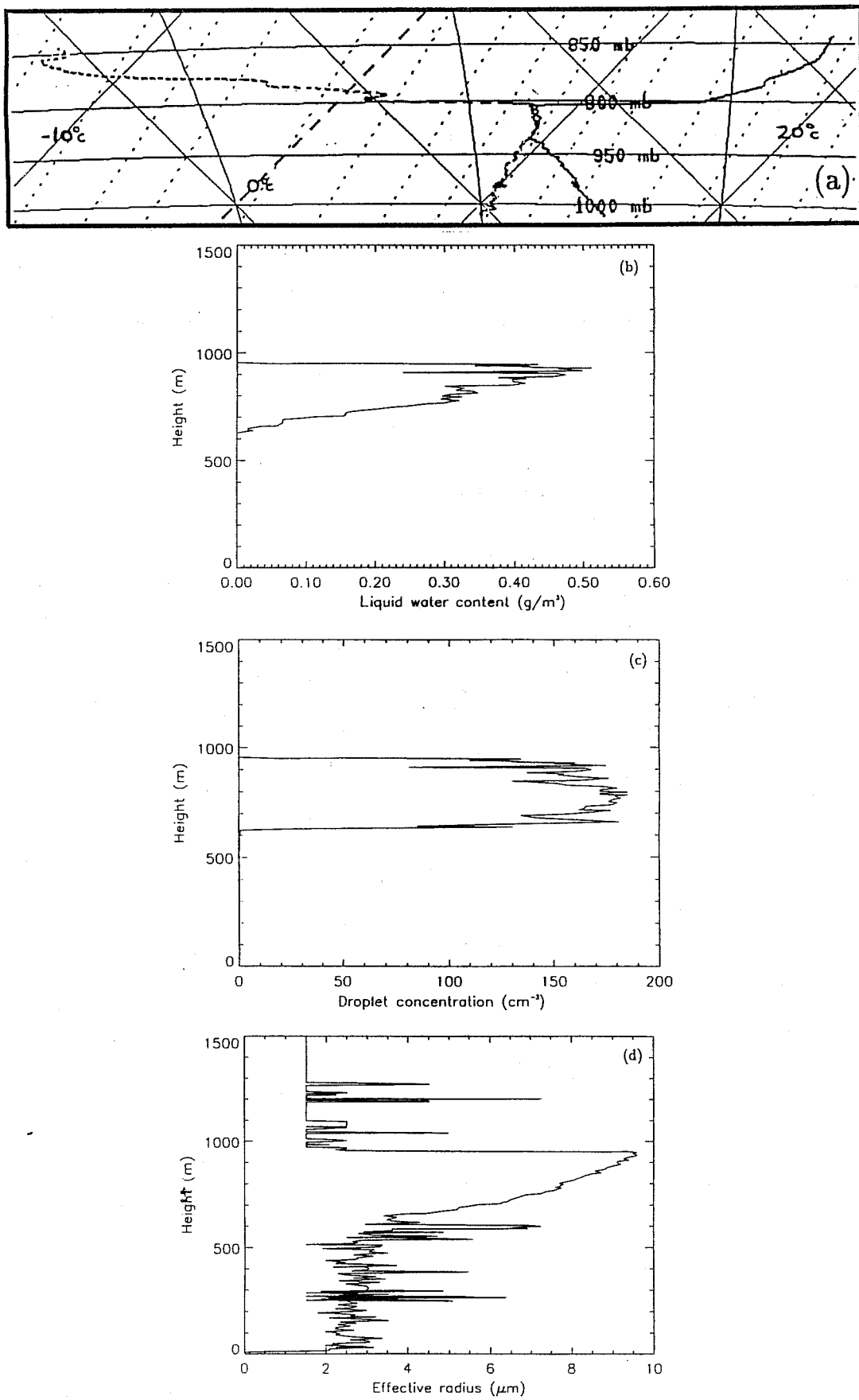


Fig. 1 Profiles obtained through a stratocumulus layer in a maritime airmass during FIRE on 3 July 1987 of (a) temperature (solid line) and dew point (dashed line) plotted on a tephigram, (b) liquid water content ($g/m^3$) as measured by the FSSP, (c) cloud droplet concentration ($cm^{-3}$) and (d) effective radius ($\mu m$) [values of $r_e$ measured when out of cloud are due to noise in the first channel of the FSSP].

by referring to the synoptic situation and deciding whether or not the air would have recently passed over land. During FIRE and FATE, relatively clean maritime airmasses were encountered since in each case the air had travelled a considerable distance over the ocean. Nearly all the airmasses in the flights around the UK, apart from a few exceptional cases, showed the effects of continental sources; even short tracks across land, such as a west to northwesterly flow over southern Ireland, considerably modified the aerosol characteristics. When typical spectra from around the UK are compared with those from off the coast of California, quite large differences are found. During ASTEX, even though the Azores are a long way from the European continent, a wide variety of airmasses was sampled. Those coming predominately from the north or north west were relatively clean, but strong east to north east outflows from Europe were found to be very polluted on several occasions. There were marked differences in the shape of the droplet spectra measured in these airmasses.

Figure 2(a) shows a typical set of averaged droplet size spectra for a layer of stratocumulus sampled during FATE in a maritime airmass. The peak concentration in the cloud remains almost constant with height but the proportion of larger droplets increases, causing a significant movement of the peak to larger radii. Thus the effective radius increases with height in cloud. A set of droplet spectra from a cloud layer sampled around the UK in a continental airmass is shown in Figure 2(b). This also shows an increase in average droplet size towards the cloud top, but the shapes of the spectra are very different from those in Figure 2(a). The peak size of the droplets at cloud top is smaller than in the maritime case, but there are still significant numbers of droplets in the larger size ranges and as a result the spectra are more skew.

The differences in spectral shape may be compared quantitatively using spectral dispersion ($d$), which is the ratio of the standard deviation $\sigma$ of the spectrum to the mean radius ($\overline{r}$), that is

$$d = \frac{\sigma}{\overline{r}}. \tag{3}$$

Figure 3 shows vertical profiles of $d$ as a function of normalised height above cloud base for the spectra given in Figures 2(a) and 2(b). The difference in spectral dispersion for the two cases can be seen clearly. It is interesting also to notice that the dispersion is approximately constant with height, which indicates that the spectrum must broaden as the mean droplet size increases. This was also observed by Nicholls and Leighton (1986).

## 4. A Parametrisation for the Effective Radius of Cloud Droplets

### 4.1 Theoretical Basis

The liquid water content can be calculated from a particular droplet size spectrum using the following equation:

$$L = \frac{4}{3}\pi\rho_w \int_0^\infty N\, r^3\, dr \tag{4}$$

where $L$ is the mass of liquid water per unit volume of air. The FSSP has 15 size channels, so this equation can be approximated by the summation:

$$L = \frac{4}{3}\pi\rho_w \sum_{n=1}^{15} r_n^3 N_n \tag{5}$$

where $N_n$ denotes the concentration of droplets in the size range $n$, $r_n$ the radius of

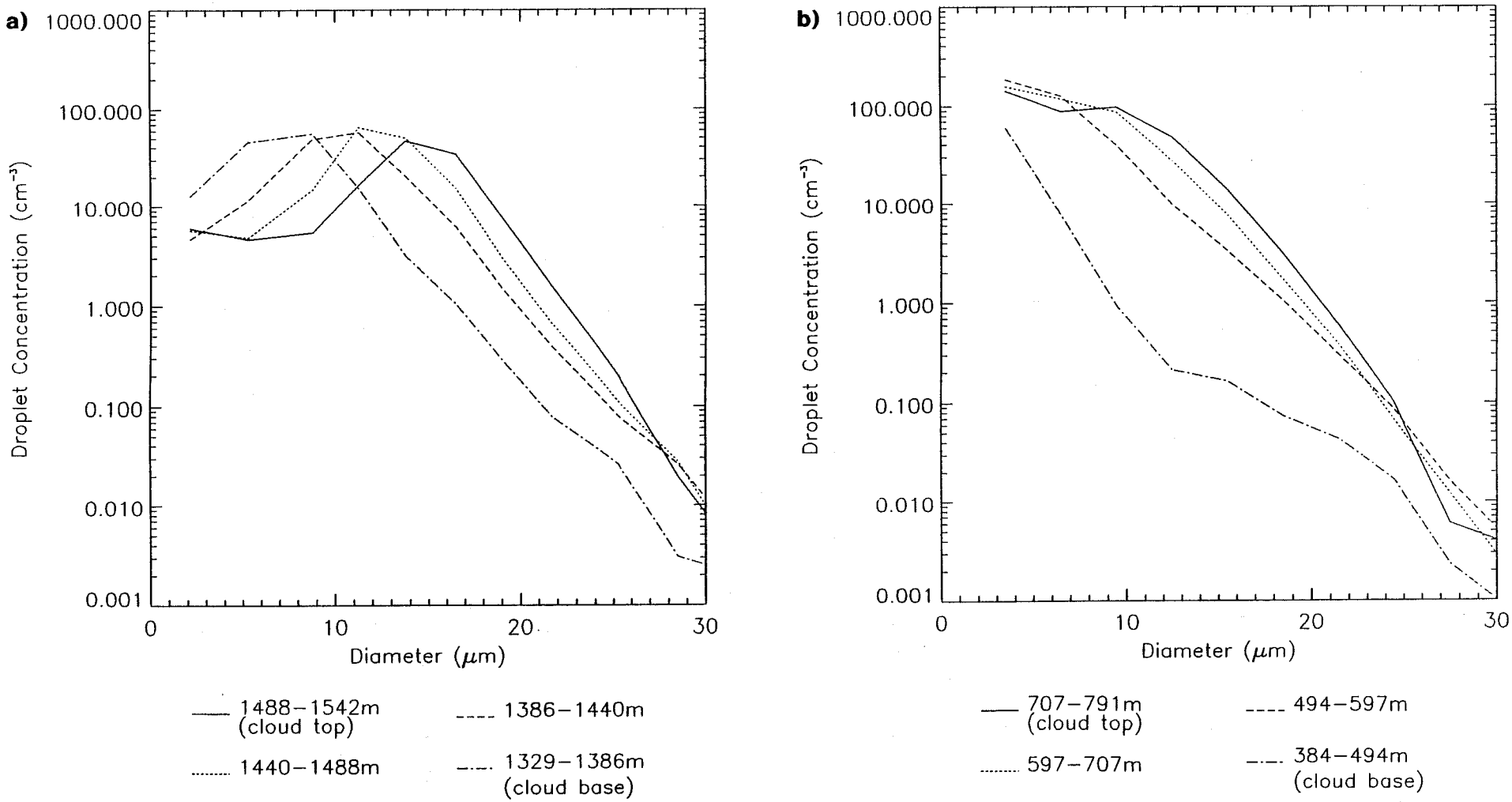


**Fig. 2** **Droplet size spectra measured by the FSSP in stratocumulus layers during profiles in (a) a maritime airmass from FATE on 6 November 1991 and (b) a continental airmass over the North Sea on 26 February 1991.**

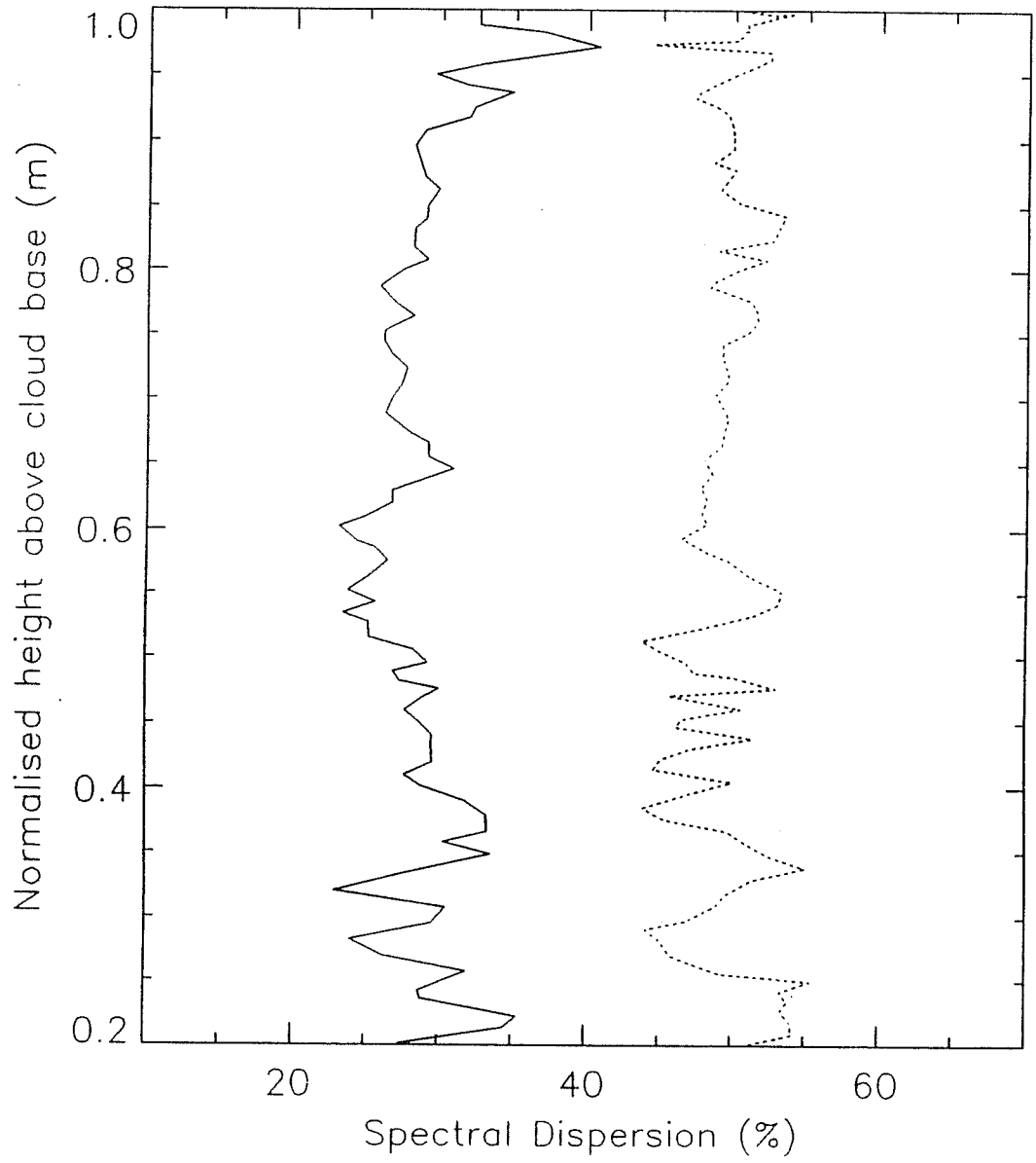


Fig. 3 A plot of spectral dispersion ($d$) against normalised height in stratocumulus cloud in a maritime airmass (solid line) during FATE on 6 November 1991 and a continental airmass (dashed line) over the North Sea on 26 February 1991.

droplets in that size range, and $\rho_w$ the density of liquid water. This can be expressed as:

$$L = \frac{4}{3}\pi\rho_w r_v^3, N_{TOT} \tag{6}$$

where $N_{TOT}$ is the total droplet concentration and $r_v$ is the mean volume radius.

### 4.2 Relationship between $r_e$ and $r_v$

If a relationship can be found between $r_e$ and $r_v$ then Eq. (6) can be used as a starting point for a parametrisation of $r_e$ in terms of the liquid water content of the cloud and the droplet concentration. Bower and Choularton (1992) compared $r_v$ with $r_e$ for a descent through stratocumulus during one of the FIRE flights and found that $r_v$ was consistently lower than $r_e$ by about $1\mu m$. However, the results presented in this paper indicate that there is a linear relationship between $r_v^3$ and $r_e^3$ in stratocumulus clouds where little entrainment is going on. That is:

$$r_v^3 = k\, r_e^3 \tag{7}$$

where $k$ is a constant.

Figure 4 shows a typical example of a scatter plot of one second averages of $r_v^3$ against $r_e^3$ measured by a FSSP in a profile through a 250m thick layer of stratocumulus. A very good straight line is found with little scatter. This particular case was for a maritime airmass studied during FIRE where the droplet sizes were large. Similar scatter plots were produced for all profiles through cloud in these experiments, and it was found consistently that $k$ varied with airmass type. In the maritime airmasses sampled in FIRE, FATE, ASTEX and around the UK, larger values of $k$ were measured than in the continental airmasses found in the vicinity of the UK and during ASTEX. This arises due to the fundamental difference in the shape of the droplet size spectra which was discussed above for the two airmass types. In continental airmasses it was found that $k = 0.67 \pm 0.07$ (1 standard deviation) while in the maritime airmasses $k = 0.80 \pm 0.07$.

It is suggested that a suitable parametrisation for effective radius is:

$$r_e = \left(\frac{3\,L}{4\,\pi\,\rho_w\,k\,N_{TOT}}\right)^{\frac{1}{3}} \tag{8}$$

The results from all the flights are summarised schematically in Figure 5, where $r_e^3$ is plotted against (FSSP liquid water content/ droplet concentration). The graph shows the envelope of all data points and they fall into two separate regions; one for continental airmasses and the other for maritime airmasses.

### 4.3 Effect of aerosol on cloud droplet concentration

#### 4.3.1 Relationship between cloud droplet concentration and aerosol concentration

Due to its transient and sub-grid scale nature cloud droplet concentration is a difficult parameter for a large scale numerical model to handle. Therefore, before Eq. (8) can be used to diagnose effective radius in models, a method for parametrising $N_{TOT}$ is required. In stratocumulus clouds, in well mixed boundary layers, the droplet concentration throughout the whole depth of the cloud is almost equal to the CCN concentration below cloud,

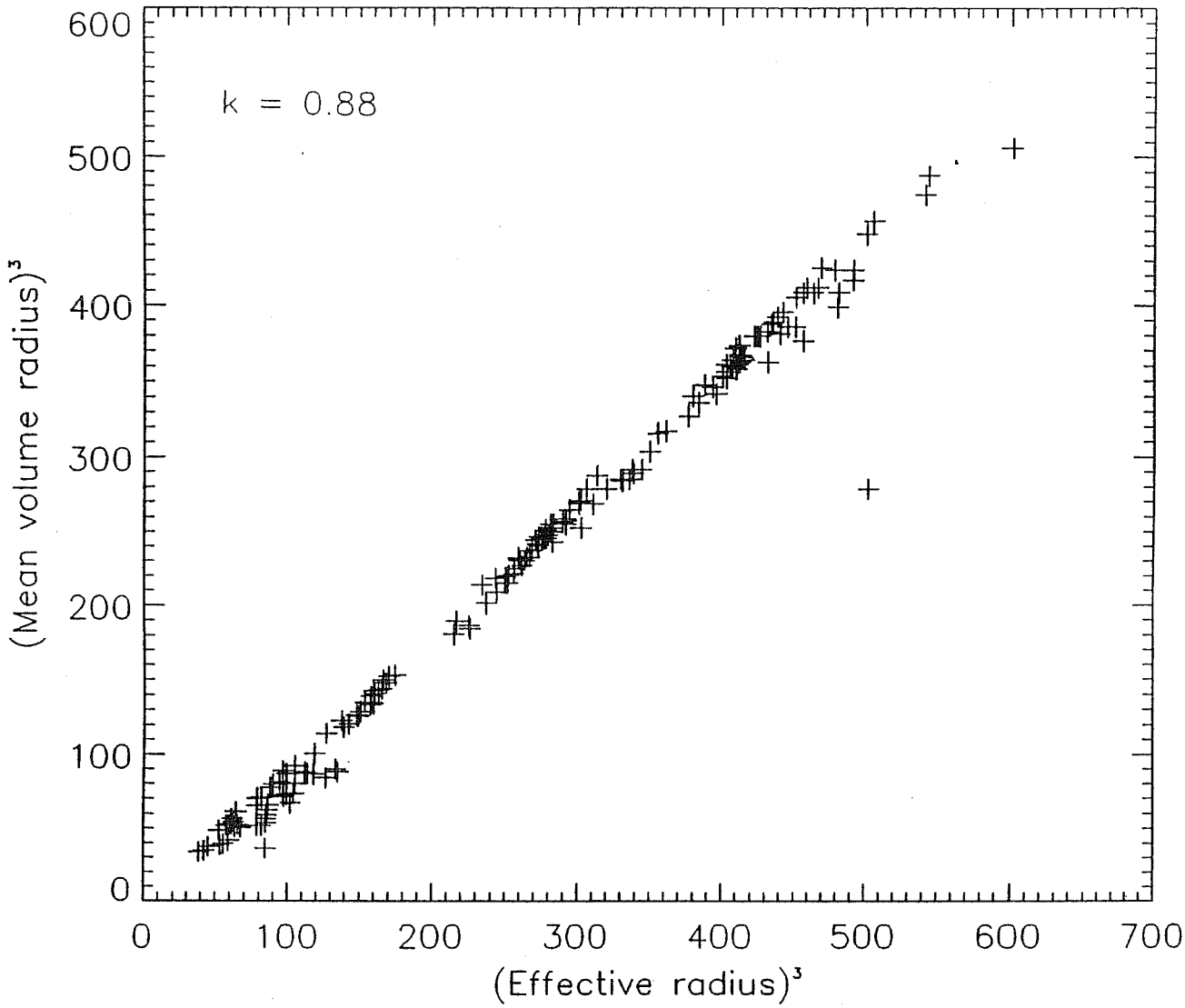


Fig. 4 Scatter plot of $r_v^3$ ($\mu m^3$) against $r_e^3$ ($\mu m^3$) for a maritime airmass cloud during FIRE on 13 July 1987.

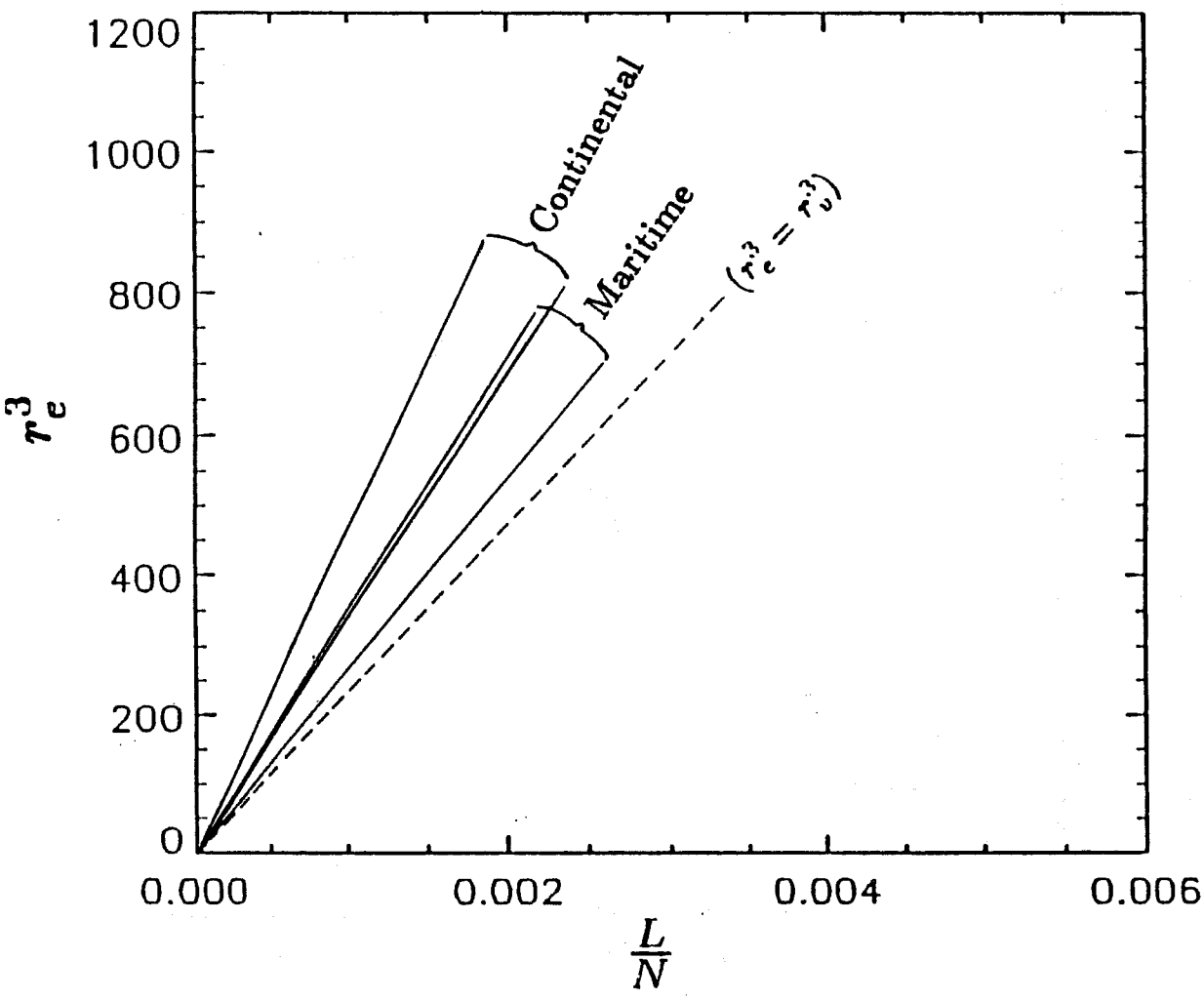


Fig. 5 Summary of the range of gradients in maritime and continental airmass clouds of $r_e^3$ ($\mu m^3$) against (liquid water content ($g/m^3$)/droplet concentration ($cm^{-3}$) for all the flights. The dashed line $R_e^3 - r_v^3$ represents $k = 1$.

and therefore in a maritime airmass it would be expected that the droplet concentration would be much less than in continental airmasses. Thus $N_{TOT}$ could be approximated by choosing a characteristic value for a given airmass. Bower and Choularton (1992) used $N_{TOT} = 600\ cm^{-3}$ over the continents and $N_{TOT} = 150\ cm^{-3}$ over the sea.

However, this simple scheme would lead to a value of $r_e$ which would often be in error, since continental type airmasses are often observed to retain their high aerosol content for some distance over the sea. As numerical models become more sophisticated it is likely that a predictive aerosol parameter will need to be included. It is well known that the concentration and chemical characteristics of aerosol particles will directly affect the concentration and maximum size of cloud droplets forming in an airmass, and hence will affect the cloud optical thickness and albedo (Twomey 1974, 1977b). Thus the inclusion of such a variable would be advantageous both from the point of view of radiation schemes and for predicting visibility. In fact, the UK mesoscale model (Golding 1990) already has the facility of including an aerosol variable, and investigations are beginning into how aerosol may be included in GCMs (Langner *et al.* 1992).

Aerosol concentration measurements taken with the PCASP during this study show that there is a good correlation between the number of aerosol just below cloud base and the cloud droplet concentration. Figure 6 summarises the aerosol concentrations measured below cloud base and the number of droplets observed in the cloud. Each point represents the average droplet concentration in a particular layer of cloud compared with the aerosol concentration measured just below the base of the layer. For the maritime airmasses there is little scatter of the points and the best fit line is close to the dashed $y = x$ line, indicating that nearly all the aerosol are good CCN and that there is very little variation in the chemical characteristics of the particles. Note that because the lower measurement limit of the PCASP is 0.05 $\mu m$ some smaller CCN may be missed, so that the aerosol concentration measured by the PCASP is probably an underestimate of the total aerosol concentration. This would account for the points which lie above the $y = x$ line. However, it is also possible that some processing or scavenging of the aerosol below cloud base by drizzle has taken place.

For the continental airmasses the scatter is much larger than for the maritime airmasses, illustrating the range of propensities to become CCN and hence the diversity of aerosol chemical characteristics amongst the airmasses sampled. The best line fit to all the data, if extrapolated to the $x$-axis, would have a positive intercept, which shows that a certain proportion of the continental particles are hydrophobic and so will not form cloud droplets. The value of this intercept will vary with the origin of the airmass; for example, an airmass of urban origin would contain a large percentage of anthropogenic aerosol particles such as carbon, which is insoluble, so the relationship between aerosol and CCN concentration for this airmass would differ from one which had, for example, originated over the desert. The best line fits suggest that $N_{TOT}$ can be parametrised in the following manner:

In maritime airmasses

$$N_{TOT} = -1.15 \times 10^{-3} A^2 + 0.963 A + 5.30 \qquad (9)$$

for values of $A$ in the range ($36 \leq A \leq 280\, cm^{-3}$), and in continental airmasses

$$N_{TOT} = -2.10 \times 10^{-4} A^2 + 0.568 A - 27.9 \qquad (10)$$

for values of $A$ in the range ($375 \leq A \leq 1500\, cm^{-3}$)

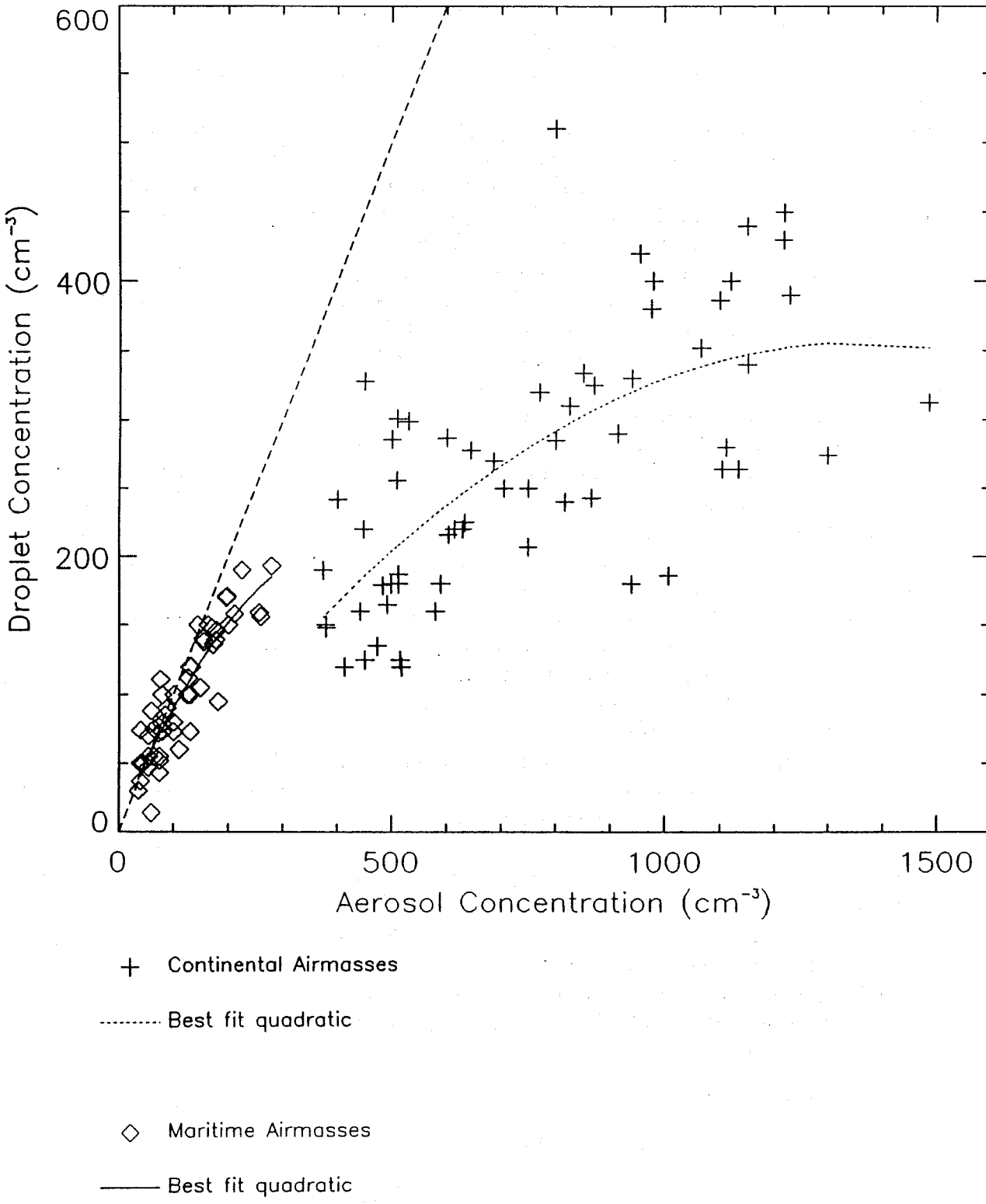


Fig. 6 Scatter plot of mean cloud droplet concentration ($cm^{-3}$) as measured by the FSSP against aerosol concentration ($cm^{-3}$) as measured by the PCASP just below cloud base for all the flights for which the PCASP was fitted. The solid line is the best fit curve for the maritime airmasses, the dotted line the best fit curve for the continental air masses and the dashed line is $y = x$.

where A is the aerosol concentration in the size range 0.05 - 1.50 $\mu m$ radius. Note that these equations are valid only over the range of observed values of $A$ to which they are fitted.

### 4.3.2 CCN Supersaturation Spectra Below Cloud Base.

The relationship between the concentration of aerosol particles below cloud base and the concentration of CCN activated into cloud droplets will, for a particular airmass composition, depend not only on the actual proportion of aerosol which are CCN, but also on the relative values of the maximum in-cloud supersaturation and the critical supersaturation of the CCN (that is, the supersaturation at which the CCN are activated). The maximum supersaturation is largely dependent on the vertical updraught velocity, and for stratocumulus clouds it is less than 0.8 % because the updraught velocities are very small, typically less than 1 $ms^{-1}$, and increases in supersaturation are rapidly reduced by condensation of water vapour onto cloud droplets. However, increases (or decreases) in the maximum supersaturation could cause increases (or decreases) in the number of CCN activated to cloud droplets within the same airmass, as illustrated by Twomey (1959). In order to investigate the variations in the maximum supersaturation between the different stratocumulus layers studied here, CCN activity spectra measured just below cloud base were used. Activity spectra, typical examples of which are given in Figure 7, show the CCN concentration activated at a particular supersaturation; this will obviously vary with the actual aerosol present. Provided there are no non-adiabatic processes occurring such as entrainment or drizzle, so that the mean droplet concentration in the cloud layer is the same as the concentration of CCN activated, it is possible to find the corresponding maximum supersaturation. Examples of CCN supersaturation spectra and the construction carried out to find the maximum in-cloud supersaturation are shown in Figure 7 for both a maritime and a continental airmass case. This procedure for calculating the maximum supersaturation was carried out for all the CCN spectra measured below cloud base during the UK, FATE and ASTEX flights (the instrument was not fitted during FIRE). Figure 8 shows how the maximum supersaturation varies from one stratocumulus sheet to another. Although there is considerable scatter in these results, they do indicate that the maximum supersaturation for stratocumulus clouds in both maritime and continental airmasses is, on average, 0.35 $\pm$ 0.13 % (1 standard deviation). This implies that given the CCN activity spectrum for an airmass in which stratocumulus clouds are forming, the cloud droplet concentration, $N_{TOT}$, could be deduced and used in Eq. (8) to find the effective radius of the cloud droplets.

## 5. Comparison with other parametrisations.

Most general circulation models use a constant value of $r_e$ for water clouds and another for ice clouds. In the UK Meteorological Office (UKMO) unified model, for example, the $r_e$ used is 7 $\mu m$ (Ingram 1990) for water clouds and 30 $\mu m$ for ice clouds. In the European Centre for Medium-range Weather Forecasts (ECMWF) operational model, a value of 15 $\mu m$ is used for water clouds (Morcrette 1990). Figure 9 shows a comparison, from the UK, FATE and ASTEX flights, of the observed $r_e$ and the predicted $r_e$ from the parametrisation detailed in Eqs. (8), (9) and (10) using measurements of the liquid water and aerosol concentration from below cloud base. The $y = x$ line is marked on and the dashed and dash-dot lines indicate the $r_e$ values that currently are being used in the UK Meteorological Office unified model and the ECMWF operational model respectively.

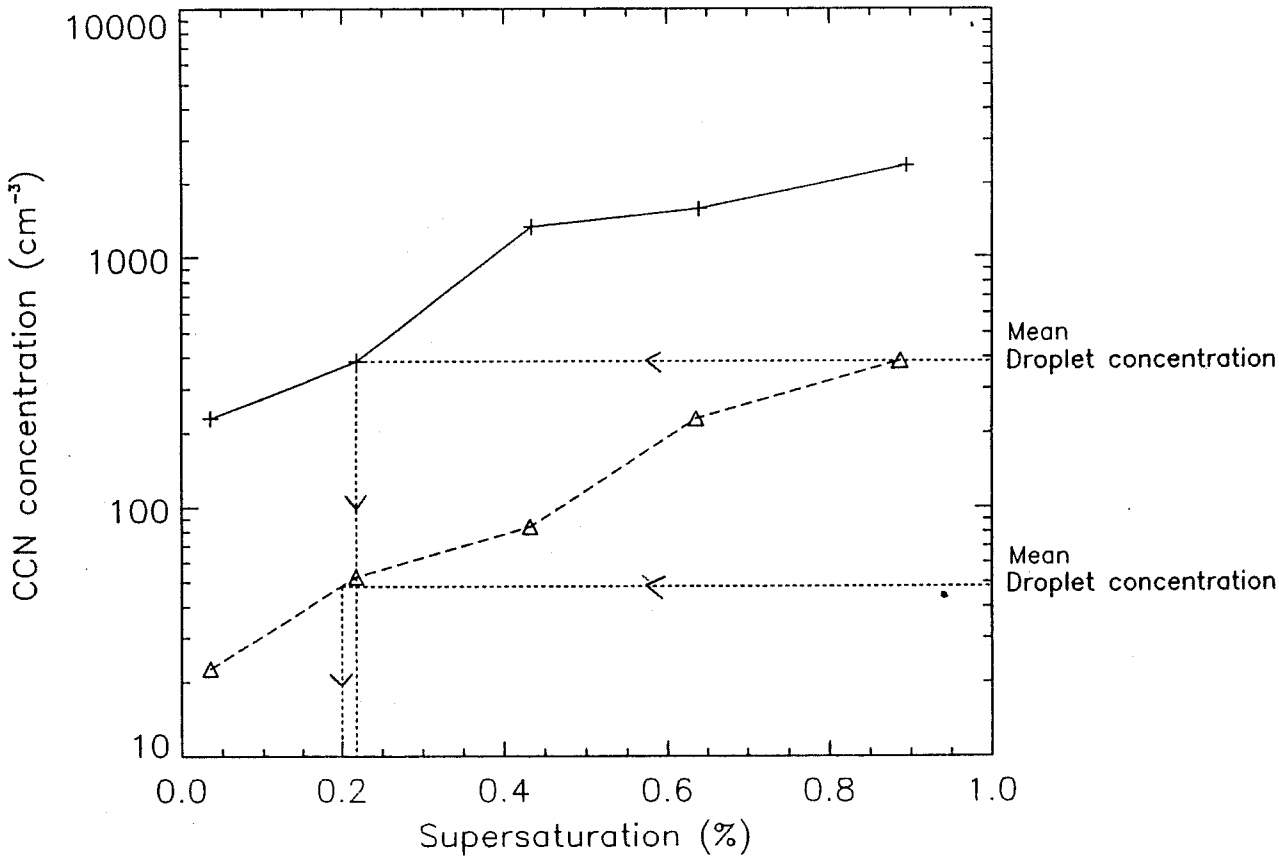


Fig. 7 CCN activity spectra measured just below cloud base in a continental airmass (solid line and crosses) during a flight over the North Sea on 7 February 1992 and a maritime airmass (dashed line and triangles) during ASTEX on 16 June 1992. The dotted line constructions show the procedure for estimating the maximum supersaturation encountered in the cloud from the mean cloud droplet concentration ($cm^{-3}$).

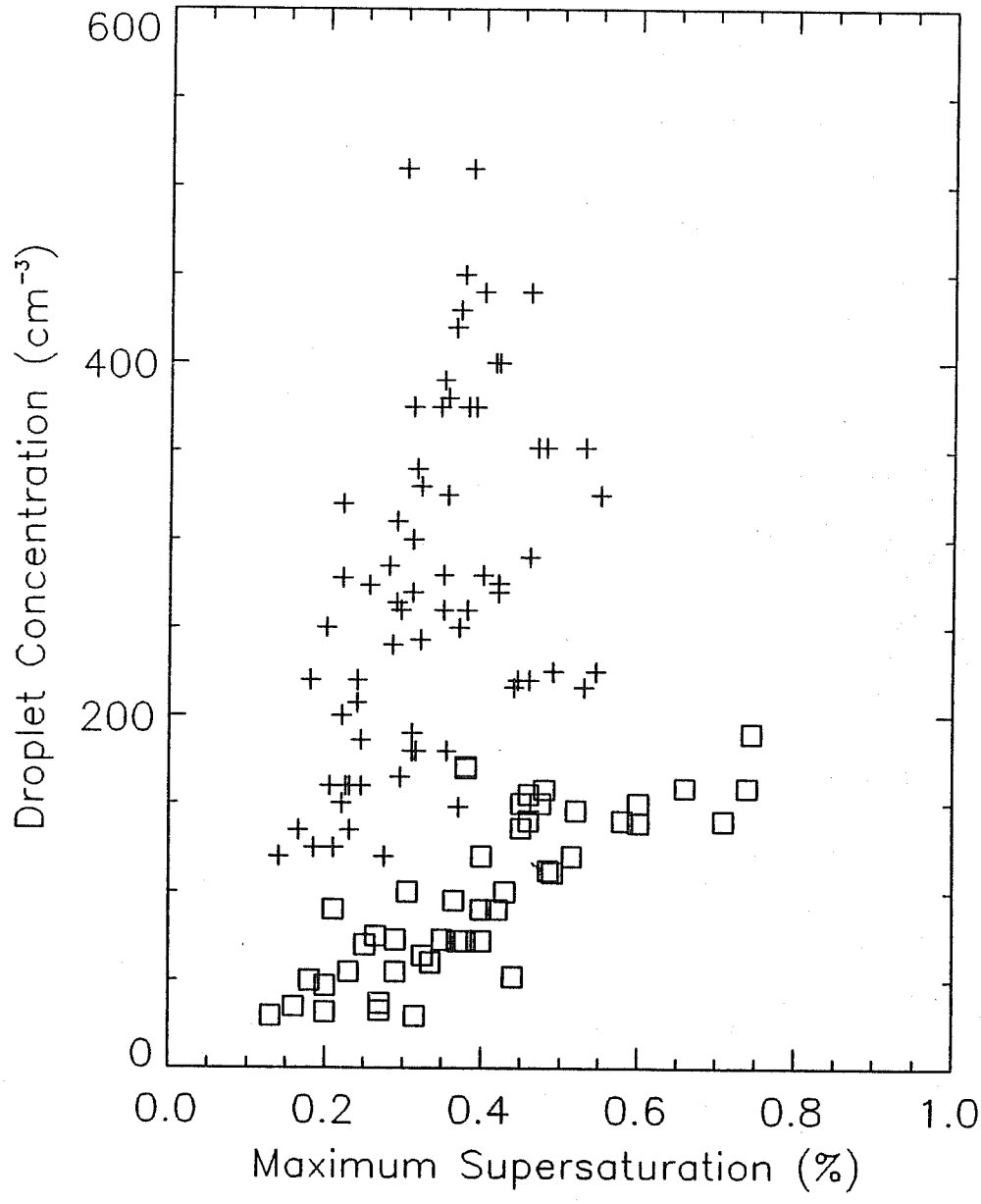


Fig. 8 Plot of cloud droplet concentration ($cm^{-3}$) against the estimated maximum supersaturation (%) for all the flights in which the CCN counter was fitted. Squares: maritime airmasses and crosses: continental airmasses.

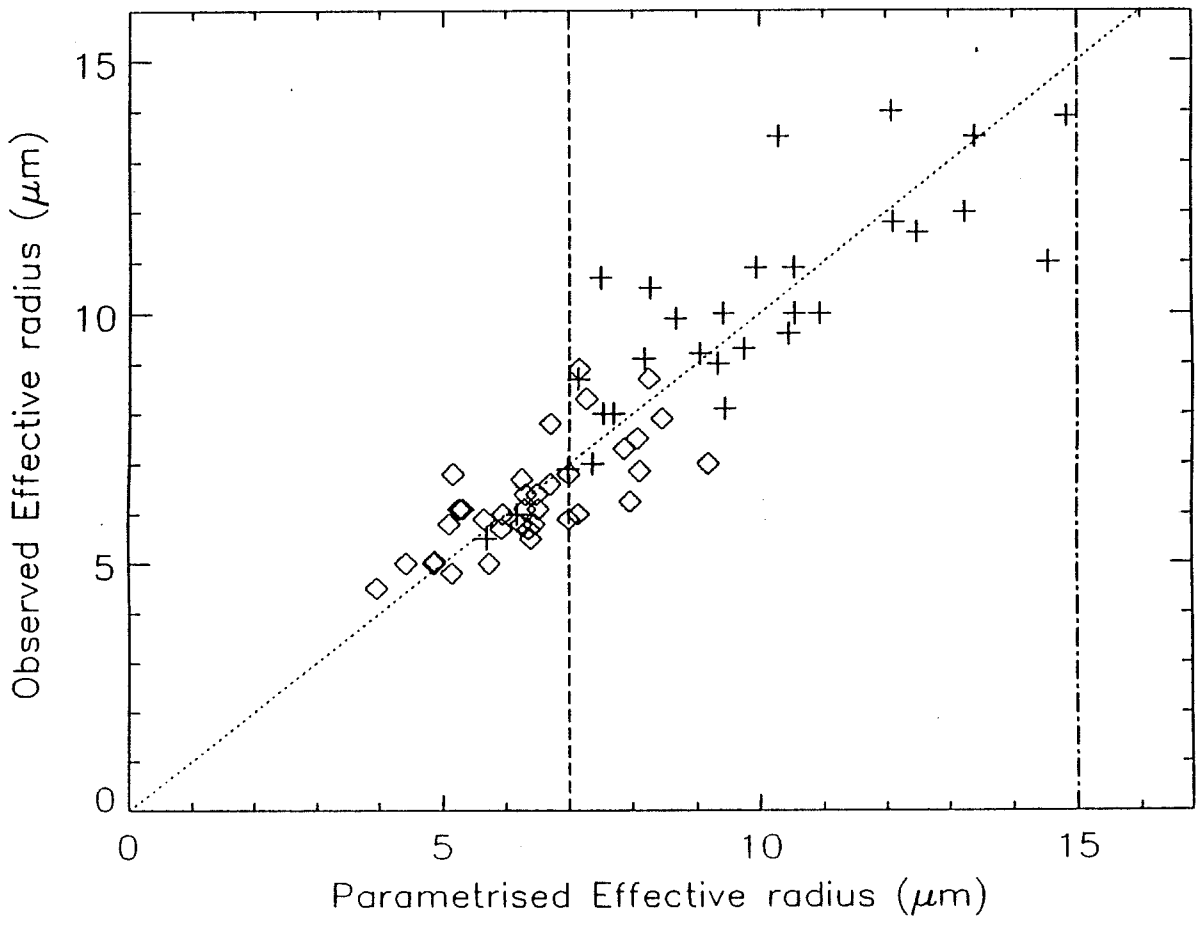


Fig. 9 A comparison of observed $r_e(\mu m)$ and the predicted $r_e(\mu m)$ from the parametrisation. Dotted line is $y = x$, the dashed line indicates the single value of $r_e$ used in the UK Meteorological Office unified model and the dash-dot line is the single value of $r_e$ used in the ECMWF operational model. Diamonds and crosses indicate continental and maritime airmass data points respectively from the FATE, ASTEX and UK experiments.

In general, the parametrisation is performing well and, as would be expected, is a much better indicator of $r_e$ than using a constant value.

The Canadian Climate Centre (McFarlane *et al.* 1992) is attempting to use a more realistic value of $r_e$ than the UKMO and ECMWF though it is still using a very simple algorithm that relates $r_e$ to the liquid water content (L), i.e.

$$r_e[\mu m] = 11L[gm^{-3}] + 4. \tag{11}$$

This expression was empirically derived by Fouquart *et al.* (1990) from "standard clouds" described by Stephens (1978*a*), which range from stratus to cumulonimbus but include cumulus and stratocumulus clouds in both maritime and continental airmasses. Figure 10(a) shows that this parametrised $r_e$ agrees well with the observed values for continental airmasses, but that $r_e$ in the maritime airmass clouds is often significantly underestimated by the parametrisation. This is likely to be the result of only allowing a dependence on liquid water content, which may be the same in two boundary layers that have different aerosol concentrations and will therefore produce clouds with different droplet sizes.

In smaller scale models, attempts have been made to parametrise $r_e$ assuming a droplet spectrum that varies with liquid water content but has a constant shape. Moeng and Curry (1990), in a large eddy simulation of stratus clouds, used a Khrgian-Mazin drop size distribution,

$$n(r) = ar^2e^{-br} \tag{12}$$

where $n$ is concentration, $r$ drop radius and $a$ and $b$ are functions of liquid water content. The $r_e$ can then be explicitly calculated i.e.

$$r_e = \frac{5}{b} \tag{13}$$

where

$$b = (2.094395 \times 10^5 N/q_l)^{\frac{1}{3}} \tag{14}$$

and

$$N = 50 + 700 \times 10^3 q_l - 300 \times 10^6 q_l^2 \tag{15}$$

In these equations, $q_l$ is liquid water mixing ratio ($kg/kg$) and $N$ is droplet concentration ($cm^{-3}$). Eq. (15) was determined empirically from observations of arctic stratus clouds. Figure 10(b) shows the comparison between the calculated $r_e$ and the observed $r_e$ and it can be seen that this parametrisation significantly underestimates the variation of $r_e$ found in our measurements. This is likely to be a result of the assumed drop size distribution, which Moeng and Curry state may be too broad for subtropical marine stratus. Also, errors may be caused by our use of this parametrisation of $N$, which is based on arctic stratus cloud data, for marine stratocumulus.

Jonas (1990) found that in a one dimensional model of the growth of droplets by condensation in an entraining warm cumulus cloud, the $r_e$ of the droplet spectrum was dependent on the CCN spectrum and the liquid water content, but was relatively insensitive to other properties of the cloud. However, Bower and Choularton (1992), when they analysed measurements of the microphysical properties of continental cumulus, small cumulus and stratiform cloud around the UK, and sub-tropical marine stratocumulus, found that the fundamental differences in entrainment processes associated with layer and convective clouds produced differences in the droplet size spectra which necessitated separate parametrisations of $r_e$ for these cloud types. They observed that in convective clouds, away from cloud base, the entrainment is strong enough that the $r_e$ varies very

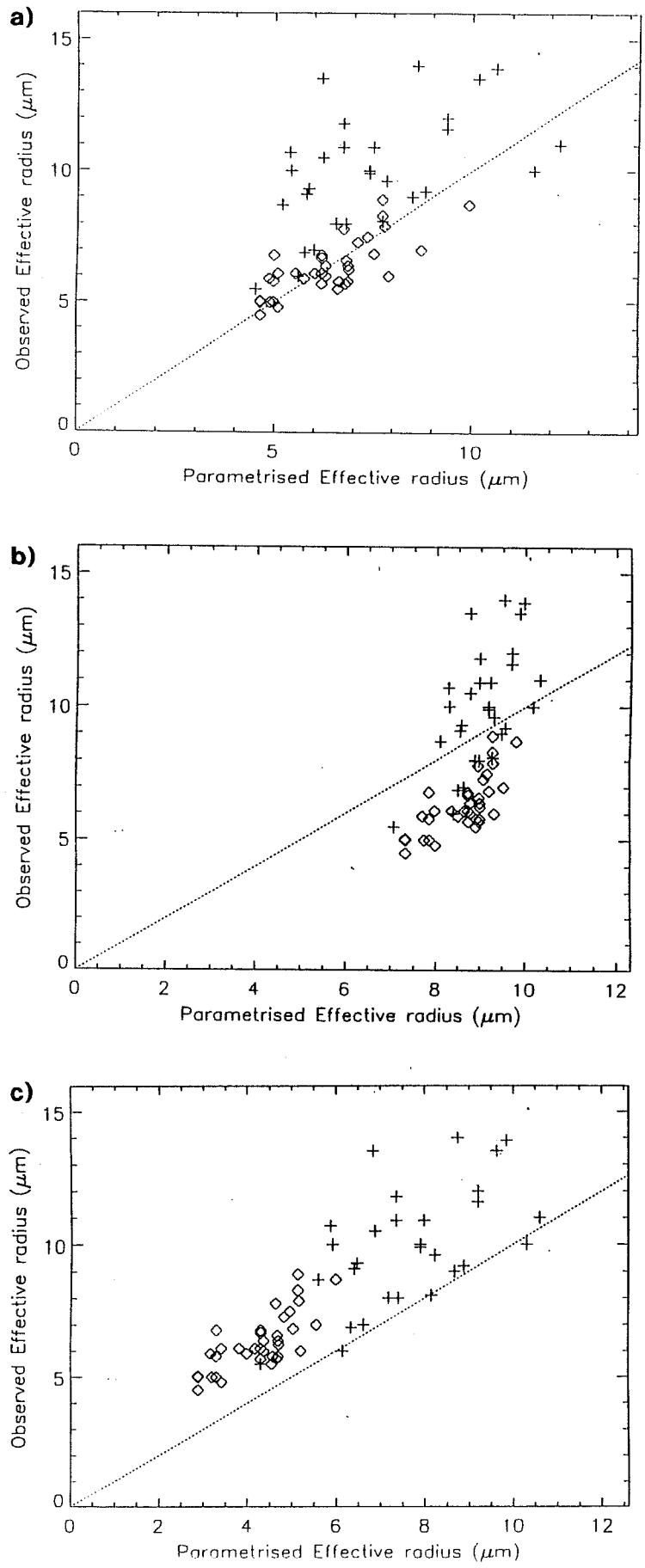


Fig. 10 Comparisons of observed $r_e(\mu m)$ with parametrisations of $r_e(\mu m)$ used by (a) the Canadian Climate Centre model, (b) Moeng and Curry and (c) Bower and Choularton. Diamonds and crosses indicate continental and maritime airmass data points respectively from the FATE, ASTEX and UK experiments.

little throughout the depth of the cloud; so it is possible to parametrise $r_e$ as a constant in cumuli which has one value over land (10 $\mu m$) and a larger value (14 $\mu m$) over the sea. For layer cloud, empirical parametrisations were produced relating $r_e$ to liquid water content and droplet concentration where the droplet concentrations were set to constant values typical of maritime and continental clouds.Figure 10(c) shows the parametrisation of Bower and Choularton (1992) for $r_e$ in stratocumulus clouds, which states that:

$$r_e = 100 \times \left(\frac{3\,L}{4\,\pi\,N}\right)^{\frac{1}{3}} \tag{16}$$

where $L$ is liquid water content in $g/m^3$ and $N$ is a fixed value of 150 $cm^{-3}$ over the oceans and 600 $cm^{-3}$ over the continents. Although all the clouds in our study were over the oceans, the continental or maritime division used throughout this paper was employed with the Bower and Choularton parametrisation. They suggest that $L$ is the liquid water content predicted by the general circulation model cloud scheme, which would be close to the adiabatic value in these clouds. For the purposes of this comparison, the measured FSSP liquid water content has been used. This parametrisation consistently underestimates $r_e$ in both types of airmass, mainly as a result of the high droplet concentration used in each case, compared with typical values measured with the FSSP in this study (see Figure 8), and also because the parametrisation assumes that $k = 1$.

## 6. Effects of cumulus on stratocumulus.

Up until now this paper has concentrated on relatively homogeneous stratocumulus layers where entrainment effects or drizzle production have had little or no effect on the characteristic shape of the droplet size spectra and $r_e^3$ has remained a linear function of $r_v^3$ throughout the depth of the cloud. The measurements show that drizzle production has very little effect in the top third of the cloud layer (Martin *et al.* 1993) and the parametrisation detailed above still holds for $r_e$ at the top of the cloud where, from the radiative transfer point of view, it is most important. However, entrainment effects, such as cloud top entrainment instability (McVean and Mason 1990) and penetration of cumulus clouds into the stratocumulus layer, do have a significant effect on the microphysical characteristics of stratocumulus and its albedo. The later, in particular, has been found to be a very common event, especially during ASTEX. This section will detail some of the microphysical interactions that can occur between cumulus and stratocumulus clouds.

### 6.1 Decoupling of the Cloud Topped Marine Boundary Layer.

Nicholls and Leighton (1986) showed that boundary layers capped by stratocumulus clouds undergo a large diurnal variation. Once a sheet of stratocumulus forms, long wave cooling from the top few meters of the cloud generates turbulent kinetic energy that forms large eddies in the vertical which transport water vapour up from the sea surface to the cloud layer and help maintain it. During the day, solar absorption by the cloud reduces the effect of the long wave cooling and the amount of kinetic energy being generated. This reduces the size of the vertical eddies and the surface becomes decoupled from the cloud and sub-cloud layer which completely cuts off the moisture supply to the cloud. Any entrainment of dry air from above the cloud will then cause the cloud to thin and perhaps break up.

Moisture can build up in the surface layer which can cause it to become conditionally unstable. When this occurs cumulus clouds form at the top of the surface layer and these

can grow and penetrate the stratocumulus. Figure 11 shows a schematic diagram of the time evolution of this process. If the boundary layer becomes deep enough, either through sea surface temperature effects or reduction in subsidence in the free troposphere, then it may remain decoupled all the time and the cumulus clouds will continue to be produced beneath the stratocumulus, even at night. This was certainly observed on many occasions during ASTEX. Figure 12 shows a profile through a boundary layer during ASTEX where the surface is decoupled from the cloud layer. The equivalent potential temperature and total water content are both higher in the surface layer than in the sub-cloud layer and they increase again in the main stratocumulus layer. Cumulus clouds were observed extensively in this flight and many were penetrating the stratocumulus layer. The cumulus clouds act as a recoupling mechanism between the surface layer and the cloud layer and may well transport enough moisture from the surface layer to the top of the boundary layer to maintain or thicken the stratocumulus. It is possible that without these cumulus clouds the stratocumulus may dissipate completely.

### 6.2 The Microphysical Interaction of Cumulus and Stratocumulus Clouds

Figure 13 shows NOAA AVHRR infra-red and visible images of a sheet of stratocumulus over the North Sea and the British Isles on the 18 May 1990. A very weak cold front had passed southwards over the North Sea and a ridge of high pressure had built behind it. This had produced a northerly flow over the North Sea which veered to a north easterly over the coast of the British Isles. Model back trajectories of the flow indicate that, for at least the previous 2 days, the air had been continuously over the sea and was therefore relatively clean. The C-130 aircraft was flying over the Wash and central North Sea. Visual observations from the aircraft and the infra-red picture indicate that the cloud top height did not vary a great deal over a very large area and the cloud was relatively extensive with only a few small holes in it. The visible image, however, shows that there are substantial variations in reflectance of the cloud sheet.

Figure 14 shows droplet concentration, effective radius, liquid water content, total water content, equivalent potential temperature and vertical velocity for two runs in a vertical stack through and just below the stratocumulus layer over the North Sea. Each is plotted against distance from the same reference point. These runs are almost over the same ground positions (although they were about 15 minutes apart), so any features sampled in the lower run can approximately be traced to the upper run. Using the flight video these runs have been annotated using observations made during the lower run, which was carried out about 100m below the main stratocumulus cloud base. During this run, several cumulus clouds were observed and penetrated, some of which were merging with the stratocumulus layer and some of which were distinctly separated from it. There were also regions where the stratocumulus base appeared to be lower and more diffuse. The graphs of the upper run in Figure 13 highlight the effects of the penetrating cumulus clouds on the stratocumulus layer. There is a sharp increase in droplet effective radius and liquid water content and a smaller but significant increase in droplet concentration, which correspond to where the cumulus clouds were observed below the stratocumulus. There are also increases in vertical velocity, liquid water content and equivalent potential temperature. These observations are typical of situations where cumulus and stratocumulus interact. The cumulus clouds act to transport surface layer air into the cloud layer and can therefore act as a moisture source for the cloud layer.

Figure 15 shows a mixing diagram of equivalent potential temperature and total water content from another example where cumulus clouds were penetrating a stratocu-

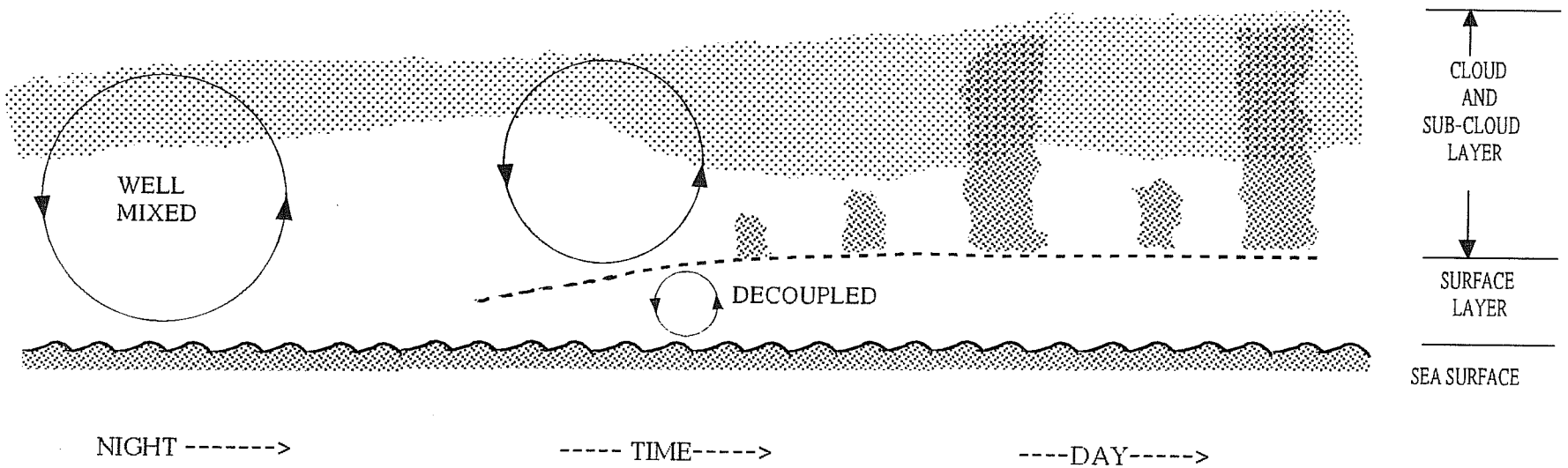


Fig. 11 Schematic diagram of the time evolution of a cloud topped marine boundary layer.

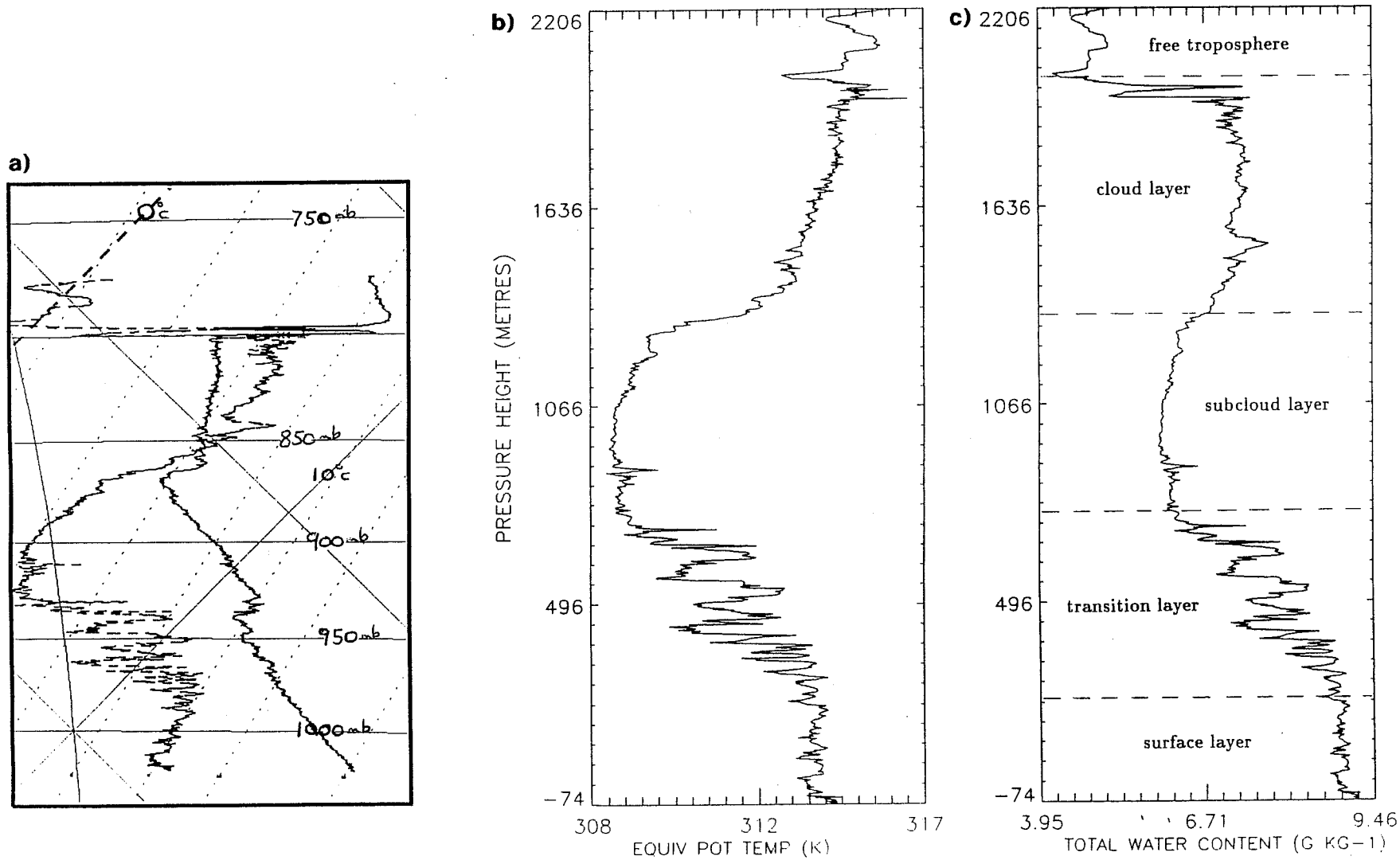


Fig. 12 Profile through a decoupled boundary layer on 19 June 1992 during ASTEX. (a) a tephigram of temperature (solid line) and dew point (dashed line); the dew point was calculated from the total water so in cloud it reads higher than the dry bulb temperature, (b) equivalent potential temperature and (c) total water content.

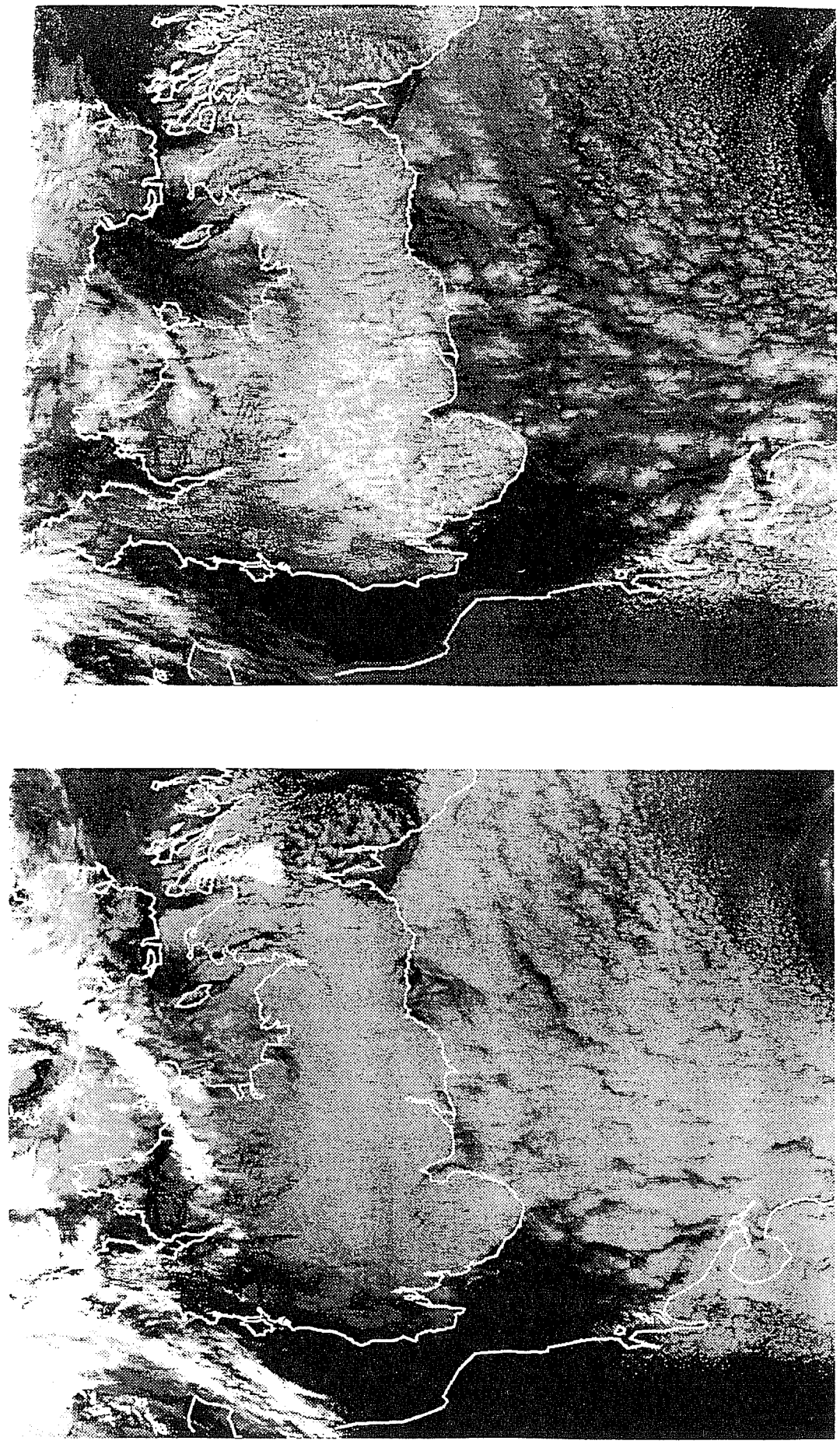

Fig. 13 Satellite images at 1315z on 18 May 1990 for (a) visible and (b) infra-red wavelengths.

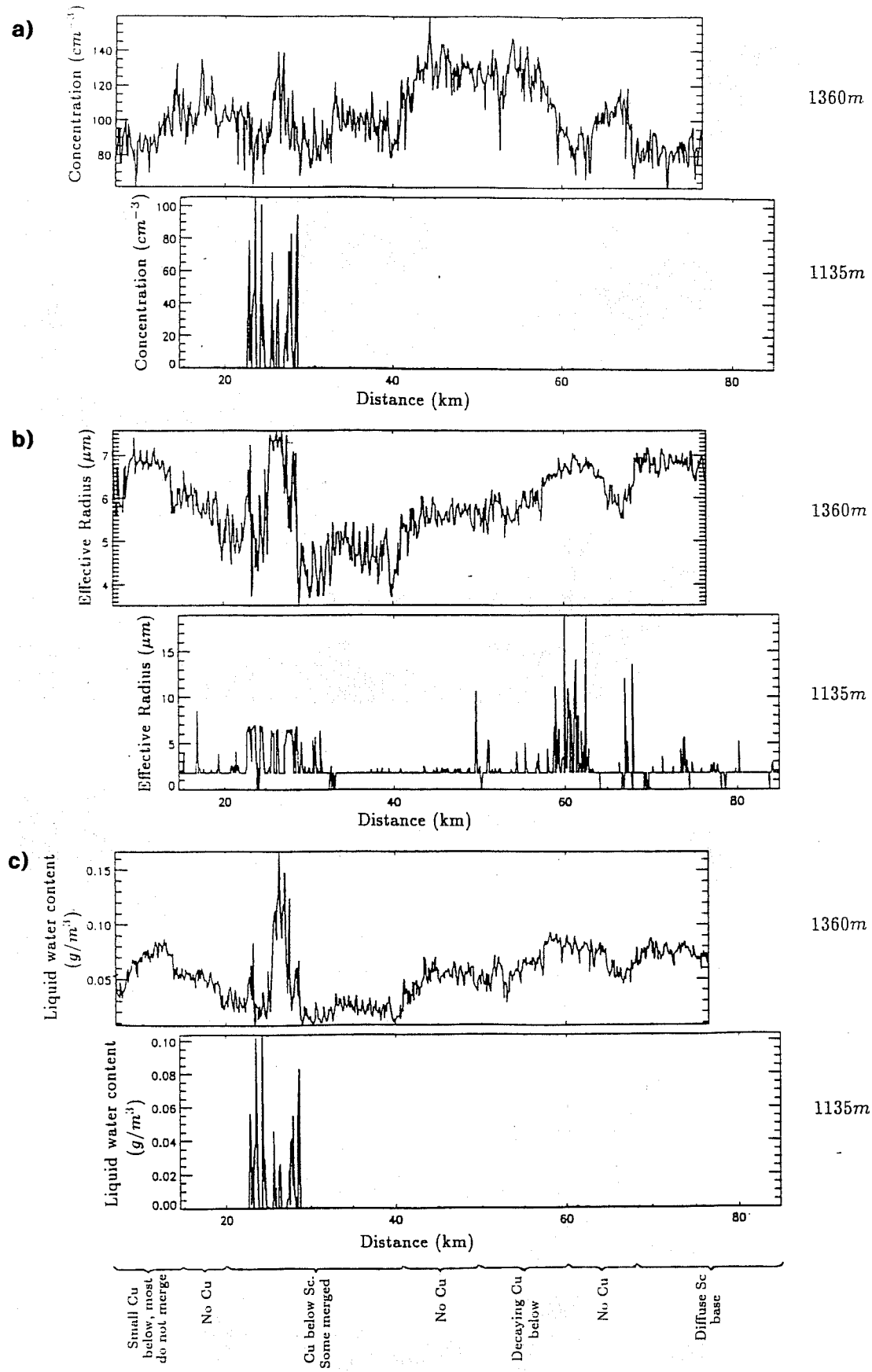


Fig. 14 Various parameters measured during two vertically stacked runs on 19 May 1990 over the North Sea. a) Droplet concentration ($cm^{-3}$) b) effective radius ($\mu m$) c) liquid water content ($g/m^3$) d) total water content ($g/kg$) e) equivalent potential temperature ($K$) f) vertical velocity ($ms^{-1}$ $g$) and h) occurrences per second of droplets $\geq 25\,\mu m$ and $\geq 150\,\mu m$ in the two runs.

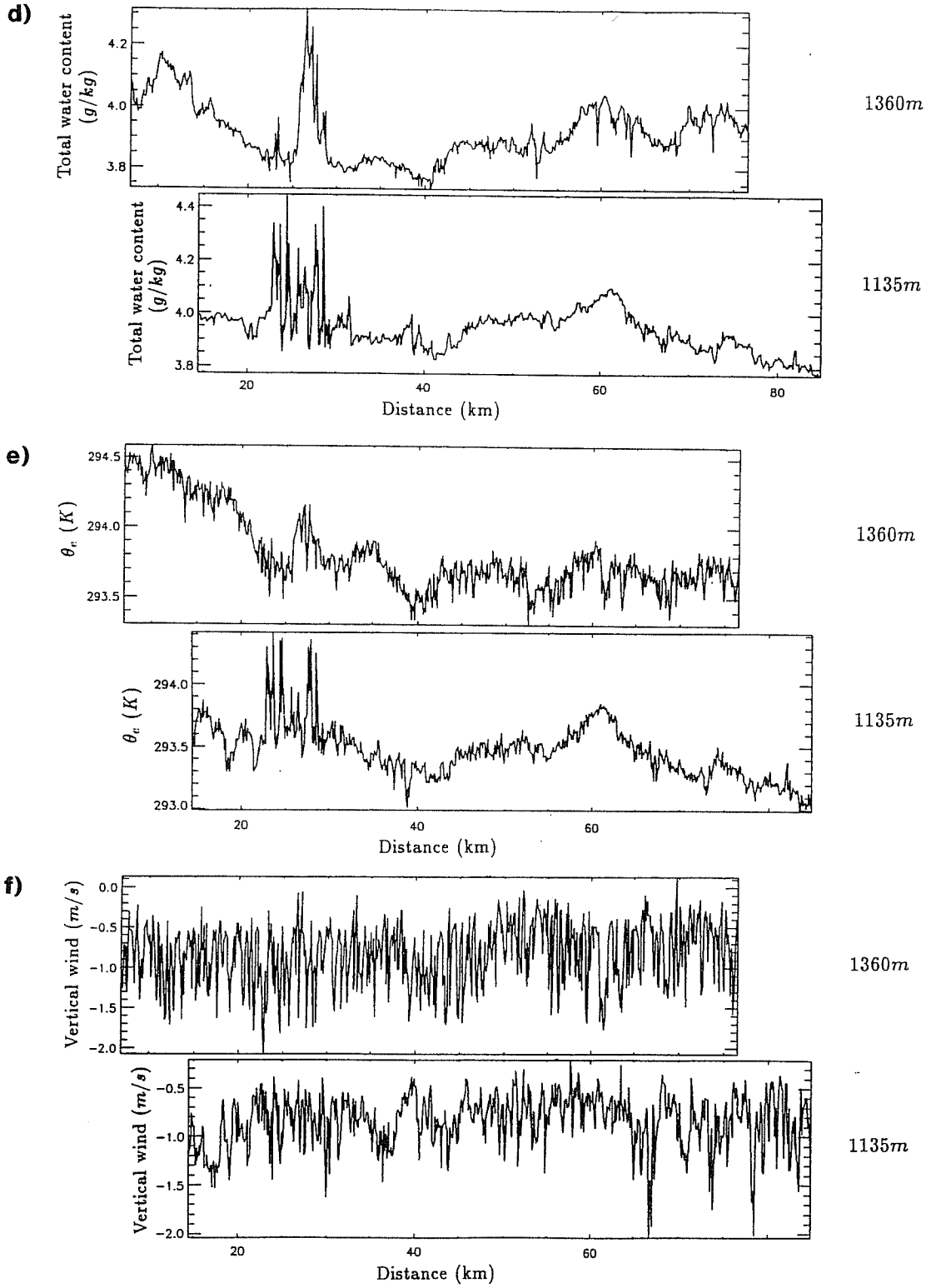


**Fig. 14 continued**

g)

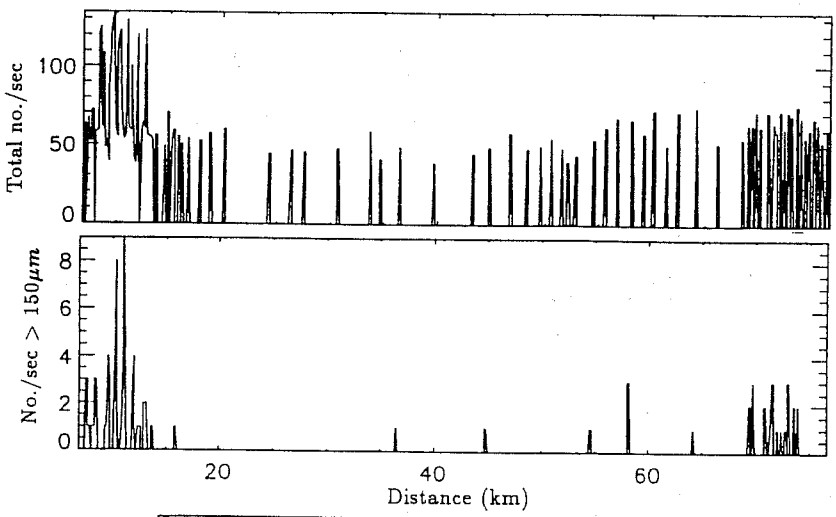


1360$m$

h)

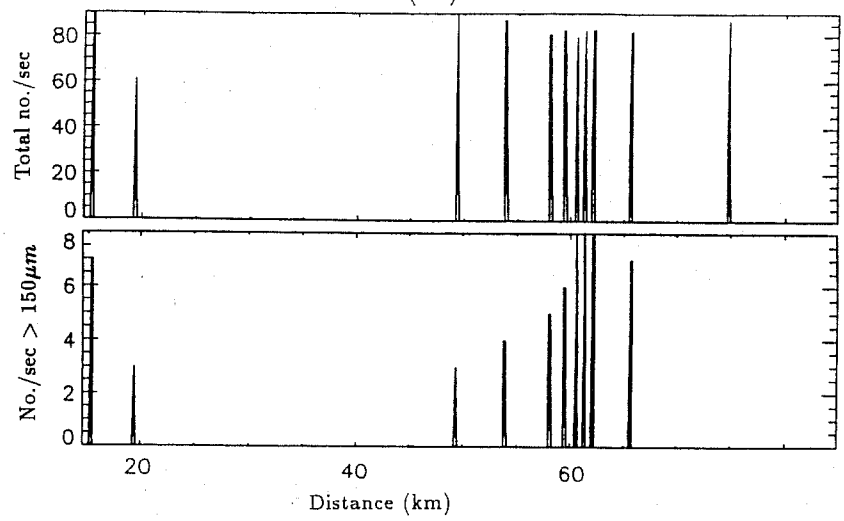


1135$m$

**Fig. 14 continued**

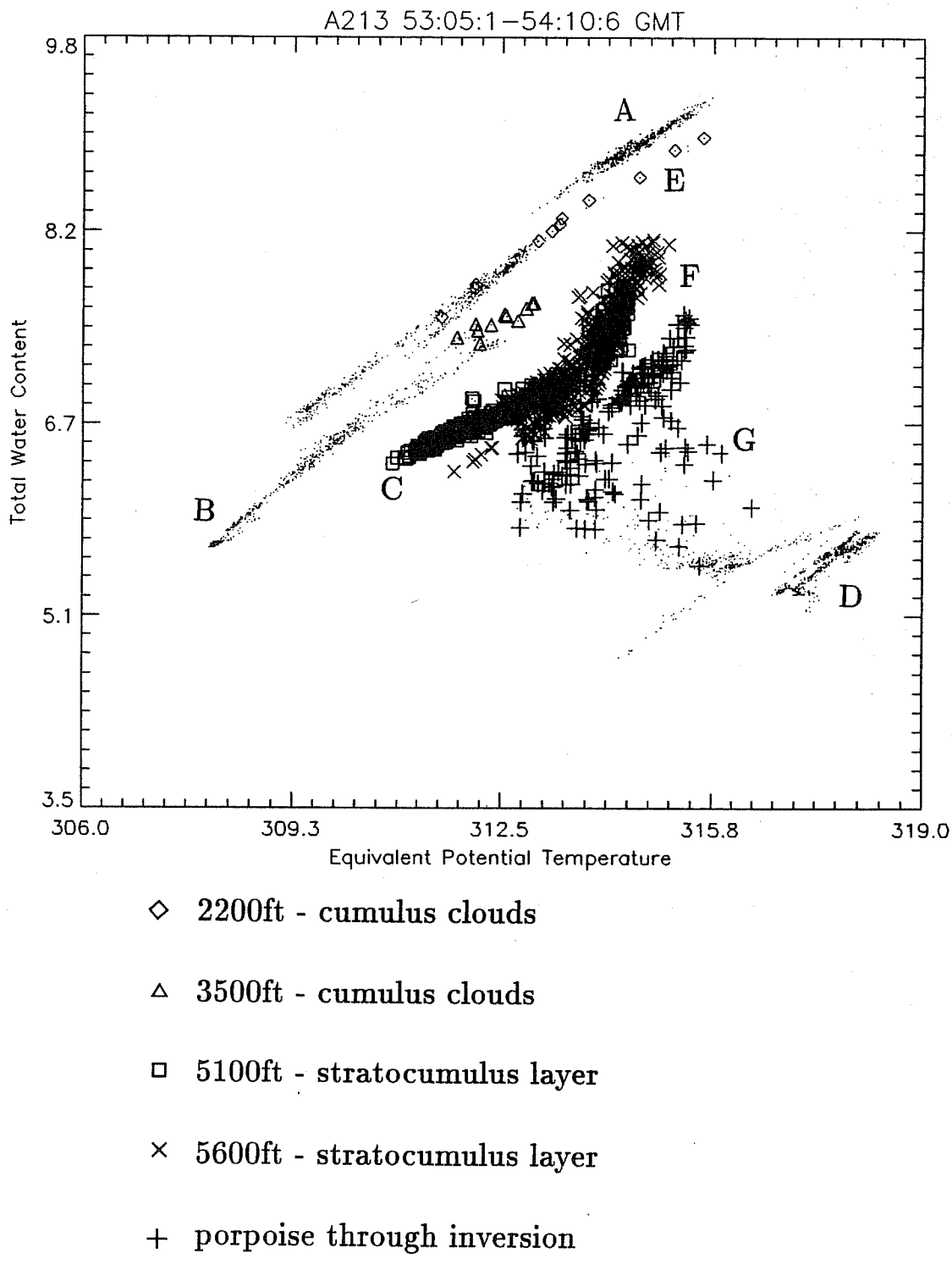


Fig. 15 Mixing diagram of total water content (*g/kg*) and equivalent potential temperature (*K*) for eight straight and level runs in a vertical stack during a flight on 19 June 1992 during ASTEX.

mulus layer on the 19 June 1992 during ASTEX (same flight as shown in Fig. 12). The dots are data points for each second during all the straight and level runs in a vertical stack. The dots are overplotted with other symbols when they are in cloud, some of which represent cumulus cells and others the main cloud layer (see key). Area A on this diagram indicates the surface layer which has high values of equivalent potential temperature and total water content, area B is the sub cloud layer, area C in the stratocumulus layer and area D the free tropospheric air. The points indicated by E are penetrations of cumulus clouds below the stratocumulus layer . These indicate that the cumulus clouds are primarily surface layer air which are entraining and mixing with the sub cloud layer air. The points indicated by F is air that has been flown through in the stratocumulus layer but that has been significantly effected by cumulus clouds penetrating the layer and mixing in a mixture of surface layer and sub cloud layer air. It is quite likely that the main stratocumulus layer has been highly modified by the cumulus clouds, the effects of which diffuse out once the cumulus cloud dies away. The points indicated by G is where parcels of air near the top of the stratocumulus layer are mixing with free tropospheric air. This is possibly coming about through enhanced mixing caused by the cumulus clouds slightly over shooting the top of the stratocumulus layer. Figure 16 shows a schematic diagram of the mixing processes that are going on in this boundary layer.

Observations show that the presence of drizzle is highly correlated with cumulus-stratocumulus interactions. Figures 14g and 14h show occurrences per second of drops greater than 25$\mu$m and the number per second which were larger than 150$\mu$m, for the runs from the flight on 18 May 1990. Comparison with Figure 14c shows that the most frequent occurrences of drizzle drops coincide not with where the most active cumuli were observed, but in regions where the stratocumulus base was extended and diffuse, and where there were decaying cumuli below. This implies that the larger drops may have developed by coalescence as a result of mixing between the two cloud types. It is likely that the now decaying cumulus clouds observed below the diffuse stratocumulus base did penetrate the stratocumulus layer and their effect has been to initiate drizzle production, which has continued after their decay.

### 6.3 Radiative effects

Changes in cloud microphysics will ultimately effect the radiative properties of the cloud layer and hence the radiation budget at the surface. Therefore if the microphysics of a stratocumulus layer is greatly affected by the penetration of cumulus clouds forming beneath the layer, and if this process is widespread, it could influence the radiation budget of the Earth as a whole.

The satellite pictures shown in Figure 13 are worthy of further comment as they illustrate quite well the multifarious effects cumulus cloud interactions can have on a stratocumulus layer. There are many localised regions of high reflectance over the sea which vary in size from a few kilometers to many tens of kilometers. Also it can be seen that the cloud layer over the land has a higher reflectance than over the sea and that this change occurs abruptly at the coast.

The measurements shown in figure 14 were made over the North Sea at approximately the same time as this satellite overpass. The spatial variation in cloud reflectance imply localised changes in cloud microphysics. An increase in reflectance may signify either a decrease in droplet effective radius or an increase in the cloud liquid water path. If both increase, then at these wavelengths the increase in the liquid water path will dominate and the reflectance will increase. The aircraft measurements indicated that when the

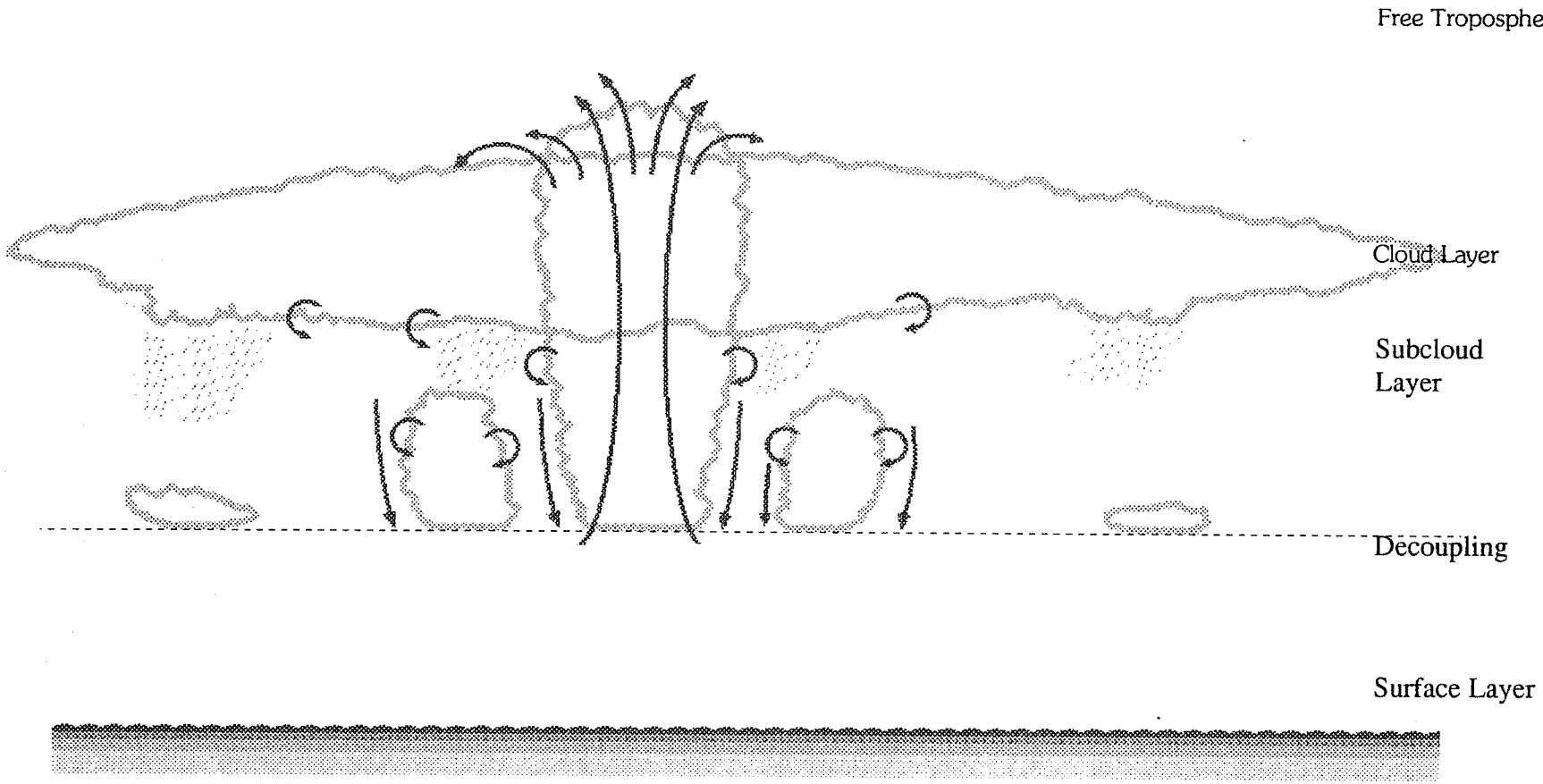


Fig. 16 A schematic diagram of the mixing processes going on in the boundary layer when cumulus clouds are interacting with a stratocumulus layer.

cumulus clouds were penetrating the stratocumulus the liquid water content and droplet effective radius were increased. It can be concluded therefore that the areas of highest reflectivity over the sea represent areas of cumulus activity. As the cumulus or patches of cumulus die away (their lifetimes are relatively short) the area of influence spreads out and is diluted through mixing processes in the stratocumulus.

It is more difficult to explain the changes in reflectance over the land as there are no in-situ measurements of the cloud microphysics there. However, some insight into the processes going on here can be gained by studying the satellite 3.7$\mu$m wavelength radiances. When the thermal signal is removed from this it is a good indicator of droplet size. Figure 17 shows the 3.7$\mu$m analysed image. The darker areas associated with cloud indicate relatively large drop size whereas the brighter areas are smaller drops.

Over the sea the cumulus cloud activity is well picked out with the most active regions having the larger droplets (see enlargement in Fig 18a). Over the land, however, the situation is quite different. The droplet sizes are much smaller and on closer inspection it can be seen there are a very large number of very small bright spots. These are particularly noticeable over East Anglia (see the enlargement in Fig 18b) and the Cheshire - Lancashire area. There are several possible reasons for the decrease in the droplet size over the land that include the following:

(a) As the moisture supply has been cut off as the air passes over the land the stratocumulus could thin. This would mean that the droplets circulating inside the cloud would not have enough time grow to the size they would over the sea and would therefore be smaller.

(b) The synoptic observations show that over the land nearly every station with cloud is reporting cumulus under a layer of stratocumulus. This implies that the boundary layer is decoupled from the cloud layer and because the surface is drier and warmer than over the sea the cumulus cloud bases will be higher and therefore the droplets in the cumulus clouds will not have enough time to grow to the sizes they achieve over the sea.

(c) The increased heating over the land has produced higher vertical velocities in the cumulus clouds which has resulted in higher supersaturations near cloud base that will cause more CCN to be activated. Therefore more droplets of a smaller size will be transported up to the stratocumulus layer.

(d) The most likely possibility is that as the air passes over the land aerosol concentrations build up in the surface layer. Then when the cumulus clouds form they transport this aerosol out of the surface layer into the cloud layer. As there are now more aerosol particles competing for an unchanged or even decreased amount of liquid water, the droplets that grow are more numerous but smaller in size. This also gives some explanation for the small bright spots on the image which could be where the active cumuli are penetrating the stratocumulus before their effects are diluted.

The direct effects of aerosol on the stratocumulus clouds can be seen clearly over the industrial areas along the east coast where large plumes of small droplets are seen being advected downwind. Even within these plumes small bright spots are observed (see enlargement in Fig. 18c) which may be due to the transport of further aerosol up from the surface layer by cumulus clouds into the plume-affected stratocumulus.

It can be seen that the effect of the cumulus clouds on the stratocumulus layer is much different over the sea than over the land. Over the sea, in the cleaner airmass, the

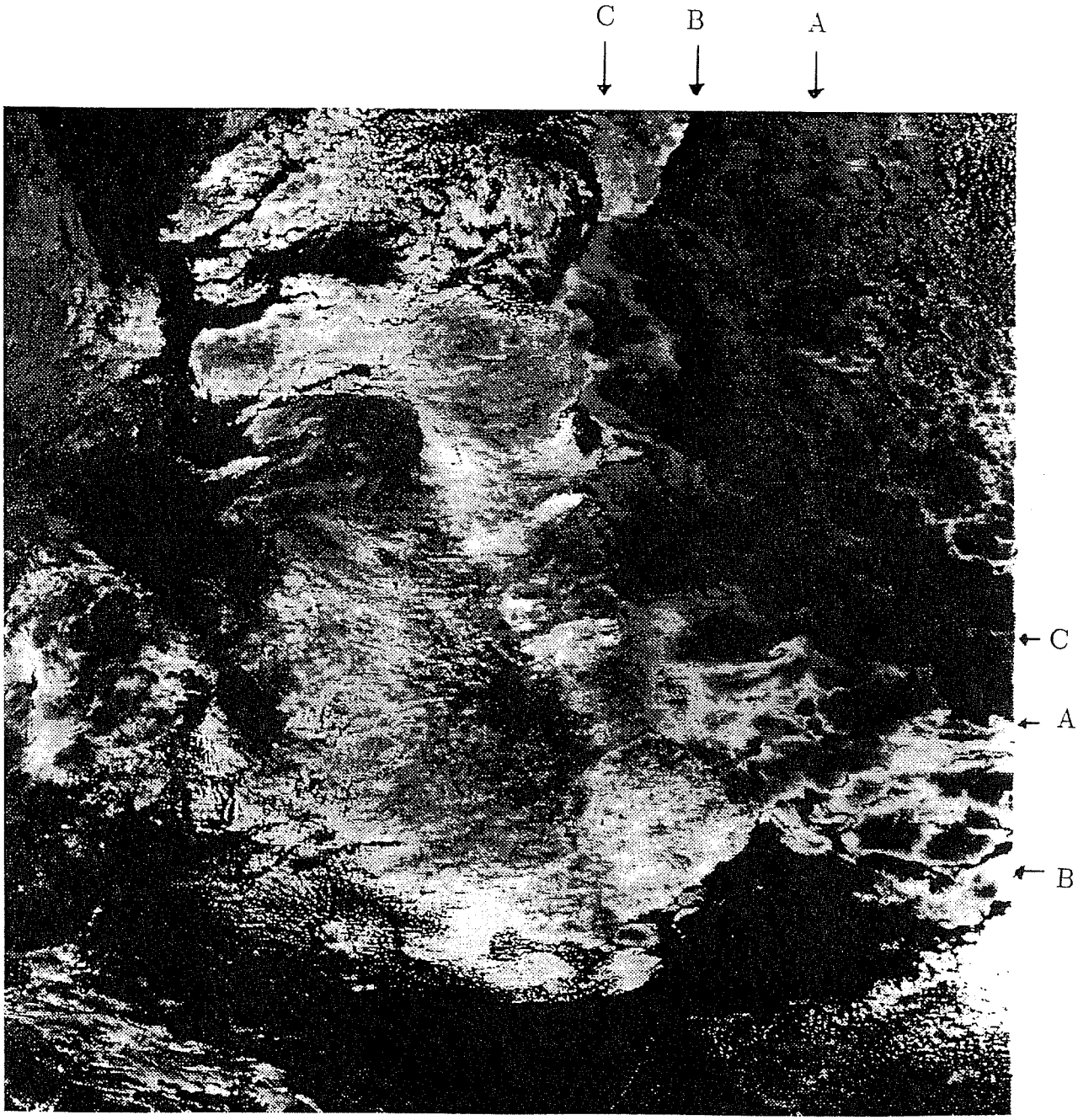


Fig. 17 3.7 $\mu m$ satellite picture at 1315z on 18 May 1990

a)

b)

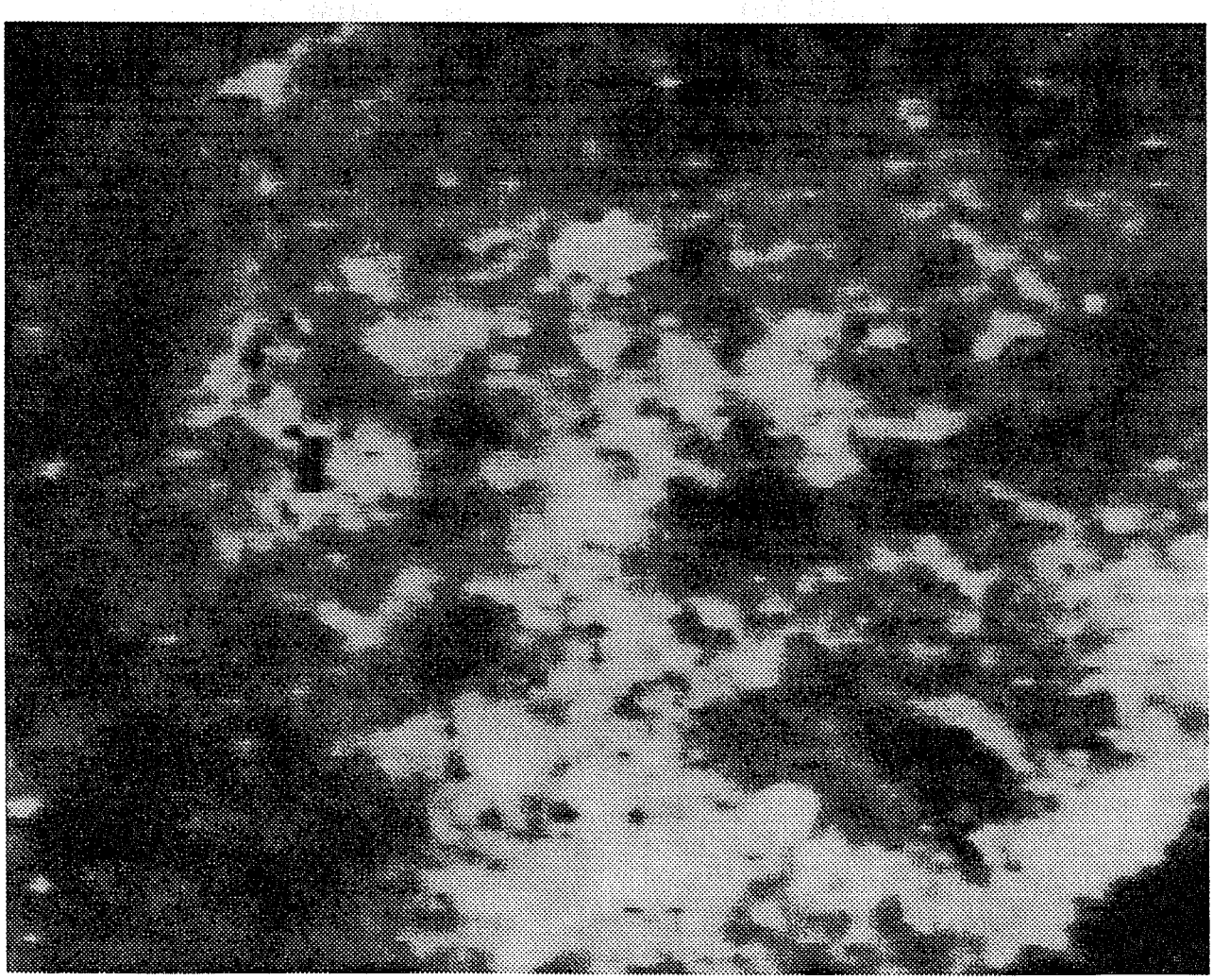

Fig. 18 Enlargements of figure 17 of areas centred on (a) AA, over the sea, (b) BB, over East Anglia and (c) CC, a plume on the east coast of the British Isles.

c)

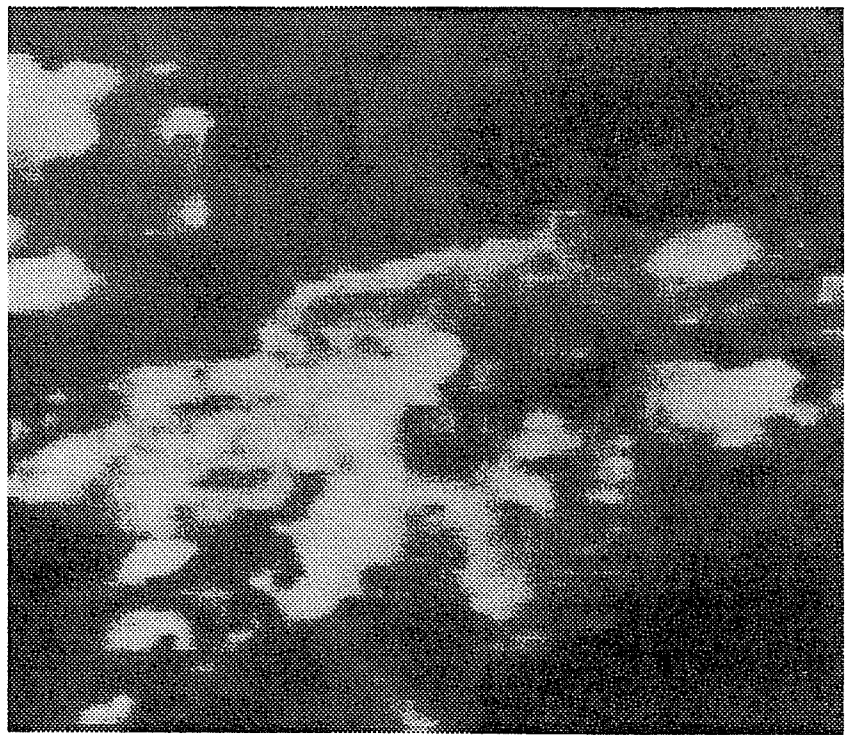

Fig. 18 continued

cumulus clouds have much larger droplets and increase the liquid water content of the stratocumulus and therefore increase the cloud reflectivity. Over the land the cumulus bases are higher so their influences on the liquid water content is less but they are transporting much higher aerosol concentrations up into the stratocumulus which is resulting in more numerous but much smaller droplets, thereby once again increasing the reflectivity of the layer.

## 7. Summary and discussion.

The measurements presented here of the microphysical properties of stratocumulus clouds and the aerosol characteristics of marine boundary layers from several regions around the globe have enabled us to produce a parametrisation of effective radius of layer clouds for radiation schemes in large scale numerical models. In general, the observations have been taken from relatively homogeneous clouds where entrainment processes such as cloud top entrainment instability and penetration by cumulus clouds are negligible or insignificant. In these circumstances, $r_e^3$ was found to be a linear function of $r_v^3$. Therefore, it has been possible to relate the $r_e$ to the liquid water content and droplet concentration in the cloud. It was also found that the droplet concentration can be parametrised in terms of the aerosol concentration if the origin of the airmass is known.

During the course of this work it was found that the most suitable parametrisation for effective radius of droplets in layer clouds is:

$$r_e(\mu m) = 10^3 \left( \frac{3\, L[g/m^3]}{4\,\pi\,\rho_w\, k\, N_{TOT}[cm^{-3}]} \right)^{\frac{1}{3}} \tag{17}$$

where the values of $k$ and $N_{TOT}$ are:

In maritime airmasses

$$k = 0.80 \pm 0.07 \text{ (1 standard deviation)}$$

$$N_{TOT} = -1.15 \times 10^{-3}\, A^2 + 0.963\, A + 5.30 \tag{18}$$

where A is the aerosol concentration in the range $(36 \leq A \leq 280\, cm^{-3})$

and in continental airmasses

$$k = 0.67 \pm 0.07 \text{ (1 standard deviation)}$$

$$N_{TOT} = -2.10 \times 10^{-4}\, A^2 + 0.568\, A - 27.9 \tag{19}$$

for values of $A$ in the range $(375 \leq A \leq 1500\, cm^{-3})$.

When entrainment effects become important, the relationship between $r_e$ and $r_v$ breaks down and such data has been ignored in the analysis.

It became clear during the course of this work that to be able to parametrise the microphysical properties of stratocumulus correctly, in particular $r_e$, the aerosol characteristics below cloud base had to be considered. Therefore we feel it is essential that more large scale numerical models start to incorporate algorithms for the prediction of advection, sources and sinks of aerosol so that the cloud-climate feedback processes can be

handled more accurately. It is also essential that models label continental and maritime airmasses in a better way. Many continental airmasses can maintain their characteristics for several days and for several thousands of kilometres once over a sea surface. This is important as clouds within continental airmasses have the potential to have much higher albedos than clouds within maritime airmasses.

The variation in the factor $k$ between maritime and continental airmass cases is caused by the fundamental difference in spectral shape. It is instructive to relate $k$ to statistical descriptions of spectral shape such as spectral dispersion and the coefficient of skewness. This may be done by writing $k$ in the form

$$k = \frac{(\overline{r^2})^3}{(\overline{r^3})^2} \tag{20}$$

using eqs. (2) and (7).

Following the method of Pontikis and Hicks (1992), $(\overline{r^2})^3$ can be expressed in terms of dispersion by expanding the equation for standard deviation:

$$\sigma = \left( \frac{1}{N_T} \int_0^\infty (r - \overline{r})^2 \, dr \right)^{\frac{1}{2}} \tag{21}$$

where $N_T$ is the total number of droplets in the spectrum, and using Eq. (3), so that:

$$(\overline{r^2})^3 = (\overline{r}^2 (1 + d^2))^3 \tag{22}$$

An expression for $(\overline{r^3})^2$ can be derived using the equation for the coefficient of skewness

$$a = \frac{1}{\sigma^3 N_T} \int_0^\infty (r - \overline{r})^3 \, dr \tag{23}$$

so that:

$$(\overline{r^3})^2 = (\overline{r}^3 (ad^3 + 1 + 3d^2))^2 \tag{24}$$

Eq. (20) can now be used to give the following expression for $k$:

$$k = \frac{(1 + d^2)^3}{(ad^3 + 1 + 3d^2)^2} \tag{25}$$

Figure 19 shows how $k$ varies with dispersion for several values of $a$. In all cases, $k$ decreases to a minimum value which is strongly dependent on $a$. The value of $d$ at which this occurs is also dependent on $a$, and is less than one for $a < 0$ and greater than one for $a > 0$. It is interesting to notice that it is possible for $k$ to be greater than one (that is, $r_v$ is larger than $r_e$), and that this will occur at successively lower values of $d$ as the skewness decreases. Also shown on the diagram are the values of $k$ for the maritime and continental airmass cases as given in Eqs. (14) and (17). Typical values of spectral dispersion measured in maritime and continental airmass cases during this study are also indicated. It can be seen that for the majority of the continental airmass cases, the coefficient of skewness is positive, and for most of the maritime cases it is negative. However, for these values of dispersion, $a = 0$ may be a fair approximation, especially since $k$ will be affected much more by changes in dispersion than changes in coefficient of skewness because of the $d^6$ terms in Eq. (25). This approximation reduces Eq. (25) to the following expression:

$$k = \frac{(1 + d^2)^3}{(1 + 3d^2)^2}. \tag{26}$$

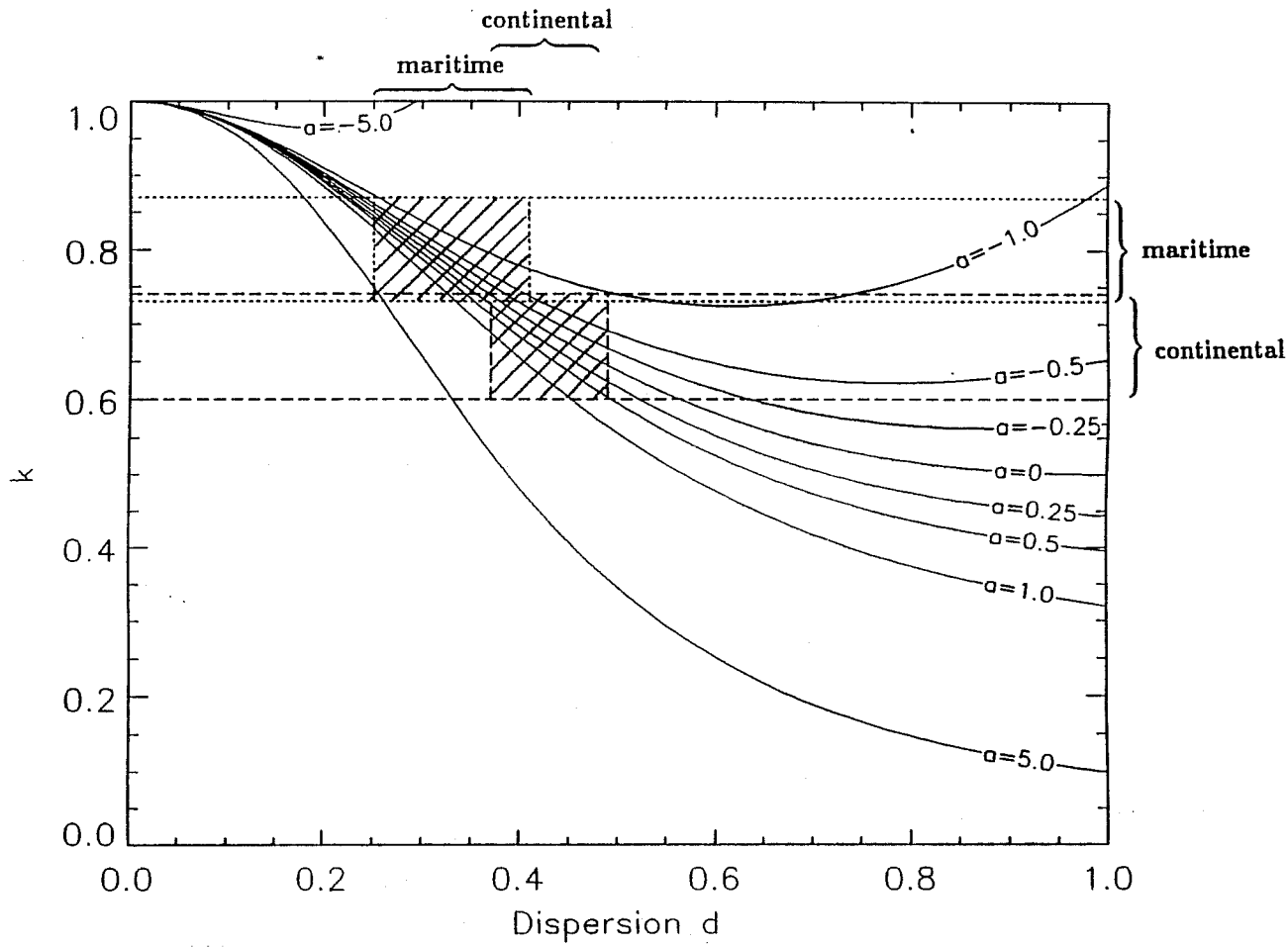


Fig. 19 A plot of the variation of *k* against dispersion (*d*) for several values of the coefficient of skewness (*a*). Shaded regions indicate the average values ± 1 standard deviation of *k* and *d* for the continental and maritime airmass clouds observed during all the experiments.

Thus, the parametrisation of effective radius given in Eq. (13) may also be written:

$$r_e = \left( \frac{3\,L(1 + 3d^2)^2}{4\,\pi\,\rho_w\,N_{TOT}\,(1 + d^2)^3} \right)^{\frac{1}{3}} \tag{27}$$

where $d = 0.33 \pm 0.08$ (1 standard deviation) for maritime airmasses, and $d = 0.43 \pm 0.06$ for continental airmasses. Figure 20 shows a comparison of observed and parametrised $r_e$ using Eq. (27). It can be seen that the assumption of $a = 0$ has only a small effect on the parametrised values compared with Figure 9, making the parametrised maritime airmass values slightly larger and the parametrised continental airmass values slightly smaller.

Pontikis and Hicks (1992) derived a parametrisation for $r_e$ in terms of spectral dispersion for use in cumulus clouds, which contains a factor $F(d)$ that is equivalent to $1/k^{\frac{1}{3}}$ and uses the assumption $\overline{(\overline{r} - r)^3} = 0$, that is, that the coefficient of skewness is zero. On applying their parametrisation to cumulus clouds measured during the JHWRP in very clean maritime airmasses, they found that $F(d)$ had an average value of 1.05, which corresponds to $k = 0.86$, and (from Figure 19) to $d = 0.24$. This is just outside the region indicated by our results for maritime airmass cases and indicates that cumulus clouds such as those sampled in JHWRP have different microphysical characteristics from the stratocumulus clouds investigated in this study, as would be expected due to the different entrainment processes taking place. However, these results imply that Eq. (17) may be used in a numerical model as a parametrisation of effective radius in stratocumulus and cumulus clouds, provided that the appropriate value of $k$ is used. Further work will be required to determine typical values of k, in for example continental cumulus clouds.

The parametrisation of the droplet concentration in layer clouds in continental airmasses is probably the weakest point of our parametrisation of $r_e$. Due to the large diversity of the chemical characteristics of the CCN and aerosol produced over the land, the degree of correlation between aerosol concentration and cloud droplet concentration is not as high as we would wish. This could be improved if more data was collected and analysed from specific continental source regions such as highly industrialized regions, deserts or arboreal areas. Then source specific parametrisations of $N_{TOT}$ could be developed and a numerical model could base its decision of which to use on the location of the source.

Up until now, very little work has been done on categorizing the chemical composition of the aerosol we have been sampling in the boundary layer. Similarly, no flights have been made in stratocumulus over land, in highly polluted airmasses where the aerosol concentration is greater than 1500 $cm^{-3}$. Future work should try to rectify this.

From satellite observations and measurements made during this work it is clear that the interaction of cumulus clouds and stratocumulus layers has a modifying effect on the reflectivity of the stratocumulus especially in the subtropics and in the late afternoon in mid-latitudes. The initial analysis of aircraft data and satellite imagery have shown that the different dynamical and entrainment processes involved with cumulus and stratocumulus clouds can lead to interactions which:

(a) increase the liquid water content in the stratocumulus layer,

(b) change the droplet size spectrum in the stratocumulus layer; this is very dependent on the aerosol concentration and type found in the surface layer, and

(c) produce drizzle.

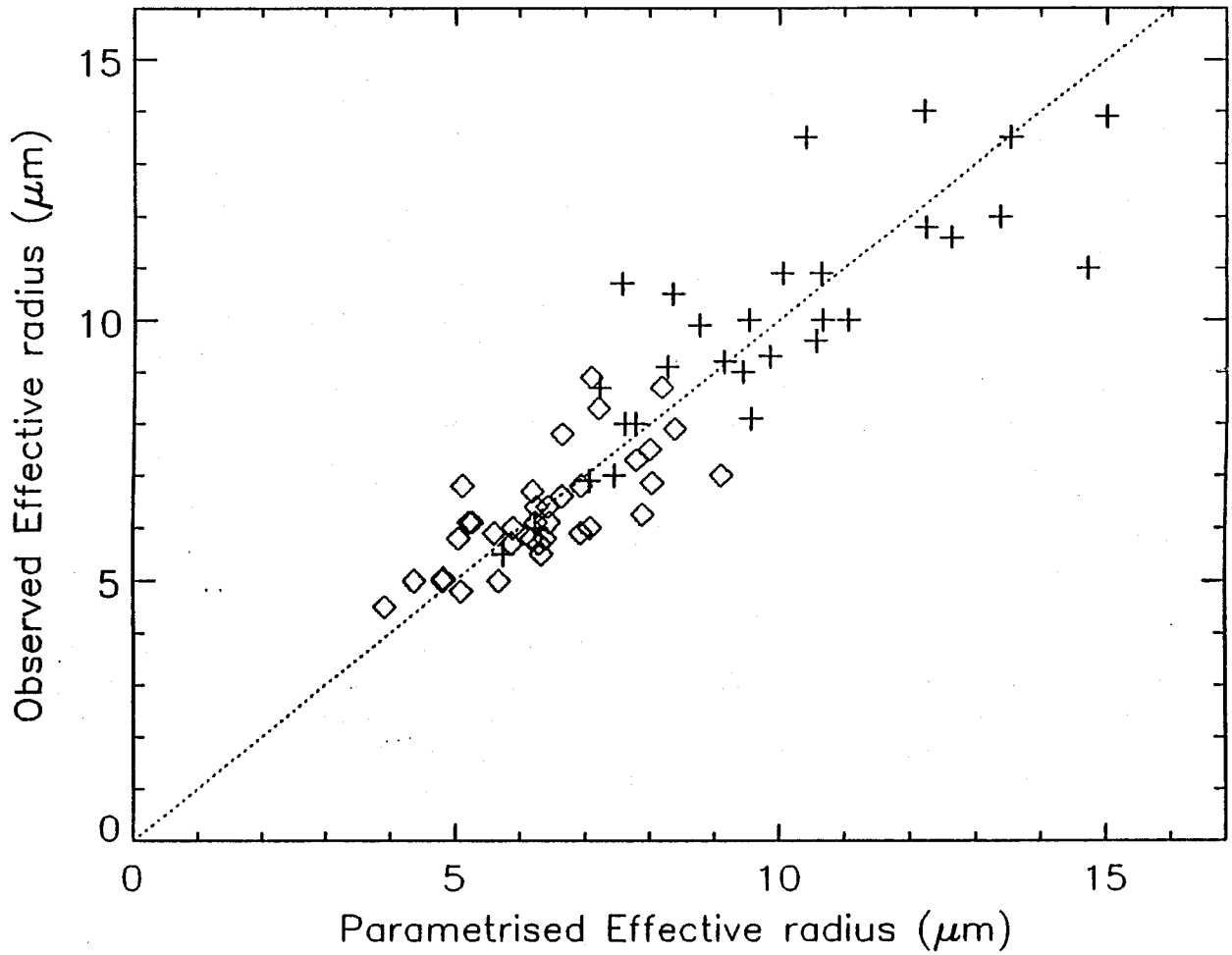


Fig. 20 Comparison of observed $r_e(\mu m)$ and parametrised $r_e(\mu m)$ assuming the coefficient of skewness of all the droplet size spectra is 0. Diamonds and crosses indicate continental and maritime airmass data points respectively from the FATE, ASTEX and UK experiments. Dotted line is $y = x$.

All three of these produce inhomogeneities in the stratocumulus layer which have significant effects on the reflectivity of the cloud top. Currently, aircraft data is being analysed to find how the interactions between cumulus and stratocumulus cloud differ in maritime and continental airmasses with a view to modifying the parametrisation of $r_e$.

**Acknowledgements** : All the data analysis reported here has been carried out in collaboration with Gill Martin of the cloud physics research group at the Meteorological Research Flight.

## REFERENCES

Albrecht, B.A., D.A. Randall and S. Nicholls, 1988: Observations of marine stratocumulus during FIRE. *Bulletin of the Amer. Met. Soc.*, **69**, 618-626

Baumgardner, D. 1983: An analysis and comparison of five water droplet measuring instruments. *J.Appl.Meteor.*, **22**, 891-910

Betts, A.K. and R. Boers, 1990: A cloudiness transition in a marine boundary layer. *J. Atmos. Sci.*, **47**, 1480-1497

Blyth, A.M. and J. Latham 1991: A climatological parameterization for cumulus clouds. *J.Atmos.Sci.*, **48**, 2367-2371

Bower, K.N. and T.W. Choularton 1992: A parametrisation of the effective radius of ice free clouds for use in global climate models. *Atmos. Res.*, **27**, 305-339

Charlson, R.J., J.E. Lovelock, M.O. Andreae and S.G. Warren, 1987: Ocean phytoplankton, atmospheric sulphur, cloud albedo and climate. *Nature*, **326**, 655-661

Curry, J.A. and G.F. Herman 1985: Infrared radiative properties of summertime arctic stratus clouds. *J.Climate and Appl. Meteor.*, **24**, 525-538

Fouquart, Y., J.C. Buriez, M. Herman and R.S. Kandel 1990: The influence of clouds on radiation: a climate-modelling perspective. *Rev. Geophys.*, **28**, 145-166

Golding, B.W. 1990: The Meteorological Office Mesoscale Model. *The Meteorological Magazine*, **119**, 81-96

Ingram, W.J. 1990: Unified model documentation paper no.23: Radiation. *Meteorological Office internal note*

Jonas, P. 1990: On the parametrization of clouds containing water droplets. *Quart.J.R.Met.Soc.*, **117**, 257-263

Langner, J., H. Rodhe, P.J. Crutzen and P.Zimmermann 1992: Anthropogenic influence on the distribution of tropospheric sulphate aerosol. *Nature*, **359**, 712-715

Martin, G.M., D.W. Johnson and A. Spice 1993: The measurement and parametrisation of effective radius of droplets in warm stratocumulus clouds. *submitted to J. Atmos. Sci.*

McFarlane, N.A., G.J. Boer, J.-P. Blanchet and M. Lazare 1992: The Canadian climate centre second-generation general circulation model and its equilibrium climate. *J.Climate*, **5**, 1013-1044

McVean, M.K. and P.J. Mason 1990: Cloud-top entrainment instability through small-scale mixing and its parameterization in numerical models. *J.Atmos.Sci.*, **47**, 1012-1030

Mitchell, J.F., C.A. Senior and W.J. Ingram 1989: $CO_2$ and climate: a missing feedback? *Nature*, **341**, 132-134

Moeng, C.-H. and J. Curry 1990: The sensitivity of large eddy simulations of a stratus topped boundary layer to cloud microphysics. *Proceedings of the San Francisco conference on cloud physics*

Morcrette, J-J. 1990: Impact of changes to the radiation transfer parametrisations plus cloud optical properties in the ECMWF model. *Mon. Wea. Rev.*, **118**, 847-873

Moss, S.J. and D.W. Johnson 1993: Aircraft measurements to validate and improve numerical model parametrisations of ice to water ratios in clouds. *(submitted to Atmos. Res.)*

Nicholls, S., 1984: The dynamics of stratocumulus: aircraft observations and comparisons with a mixed layer model. *Quart.J.R.Met.Soc.*, **110**, 783-820

Nicholls, S. and J. Leighton, 1986: An observational study of the structure of stratiform cloud sheets: Part I. Structure. *Quart.J.R.Met.Soc.*, **112**, 431-460

Pontikis, C.A. and E.M. Hicks 1992: Contribution to the cloud droplet effective radius parametrisation. *Geophys. Res. Lett.*, **19**, 2227-2230

Pruppacher, H.R. and J.D. Klett 1980: *Microphysics of clouds and precipitation.* D.Reidel Holland

Randall, D.A., J.A. Coakley Jr, C.W. Fairall, R.A. Kropfli and D.H. Lenschow 1984: Outlook for research on subtropical marine stratiform clouds. *Bull. Amer. Meteor. Soc.*, **65**, 1290-1301

Rogers, D.P., D.W. Johnson and C.A. Friehe 1993: The stable internal boundary layer over a coastal sea. I: Airborne measurements of the mean and turbulence structure. *(submitted to J. Atmos. Sci.)*

Saxena, V.K. and J.L. Kassener Jr. 1970: Thermal diffusion chambers as cloud nuclei counters. *Proceedings of the U.S. Atomic Energy Commission symposium on precipitation scavenging.*

Schmetz, J., A. Slingo, S. Nicholls and E. Raschke, 1983: Case studies of radiation in the cloud-capped atmospheric boundary layer. *Phil. Trans. R. Soc. Lond.*, **308**, 377-388

Slingo, A. and H.M. Schrecker 1982: On the shortwave radiative properties of stratiform water clouds. *Quart.J.R.Met.Soc.*, **108**, 407-426

Slingo, A. 1990: Sensitivity of the earth's radiation budget to changes in low clouds. *Nature*, **343**, 49-51

Stephens, G.L. 1978*a*: Radiation profiles in extended water clouds. I: Theory. *J.Atmos.Sci.*, **35**, 2111-2122

Stephens, G.L. 1978*b*: Radiation profiles in extended water clouds. II: Parametrization schemes. *J.Atmos.Sci.*, **35**, 2123-2132

Strapp, J.W., W.R. Leaitch and P.S.K. Liu 1992: Hydrated and dried aerosol-size-distribution measurements from the Particle Measuring Systems FSSP-300 probe and the deiced PCASP-100X probe. *J.Atmos.Oceanic Technol.*, **9**, 548-555

Taylor, K.E. and S.J. Ghan 1992: An analysis of cloud liquid water feedback and global climate sensitivity in a general circulation model. *J.Climate*, **5**, 907-919

Twomey, S. 1959: The nuclei of natural cloud formation: the supersaturation in natural clouds and the variation of cloud droplet concentrations. *Geophys. Pura et appl.*, **43**, 243-249

Twomey, S. 1974: Pollution and the planetary albedo. *Atmos. Environ.*, **8**, 1251-1256

Twomey, S. 1977a: The influence of pollution on the shortwave albedo of clouds. *J. Atmos. Sci.*, **34**, 1149-1152

Twomey, S.A., 1977b: *Atmospheric aerosols.* Elsevier